UNIVERSIDADE ESTADUAL DE CAMPINAS

INSTITUTO DE QUÍMICA

MATHEUS BATISTA CORDEIRO DE SOUZA

STUDY OF GLYCEROL ELECTROOXIDATION ON PLATINUM AND GOLD SURFACES MODIFIED BY METAL ADATOMS

ESTUDO DA ELETRO-OXIDAÇÃO DE GLICEROL EM SUPERFÍCIES DE PLATINA E OURO MODIFICADAS POR ADÁTOMOS METÁLICOS

CAMPINAS
2018

MATHEUS BATISTA CORDEIRO DE SOUZA

STUDY OF GLYCEROL ELECTROOXIDATION ON PLATINUM AND GOLD SURFACES MODIFIED BY METAL ADATOMS

ESTUDO DA ELETRO-OXIDAÇÃO DE GLICEROL EM SUPERFÍCIES DE PLATINA E OURO MODIFICADAS POR ADÁTOMOS METÁLICOS

Dissertação de Mestrado apresentada ao Instituto de Química da Universidade Estadual de Campinas como parte dos requisitos exigidos para a obtenção do título de Mestre em Química na área de Físico-Química

Master's thesis presented to the Institute of Chemistry of the University of Campinas as part of the requirements to obtain the title Master's in Chemistry in the area of Physical Chemistry

Supervisor: Prof. Dr. Pablo Sebastian Fernandez

ESTE EXEMPLAR CORRESPONDE À VERSÃO FINAL DA DISSERTAÇÃO DEFENDIDA PELO ALUNO MATHEUS BATISTA CORDEIRO DE SOUZA, E ORIENTADA PELO PROF. DR. PABLO SEBASTIAN FERNANDEZ

CAMPINAS
2018

Agência(s) de fomento e nº(s) de processo(s): FUNCAMP
ORCID: https://orcid.org/0000-0003-4785-3839

Ficha catalográfica
Universidade Estadual de Campinas
Biblioteca do Instituto de Química
Camila Barleta Fullin - CRB 8462

So89e

Souza, Matheus Batista Cordeiro de, 1992-
Study of glycerol electrooxidation on platinum and gold surfaces modified by metal adatoms / Matheus Batista Cordeiro de Souza. – Campinas, SP : [s.n.], 2018.

Orientador: Pablo Sebastian Fernandez.
Dissertação (mestrado) – Universidade Estadual de Campinas, Instituto de Química.

1. Glicerol. 2. Eletro-oxidação. 3. Adátomos metálicos. 4. Cromatografia líquida de alta eficiência. 5. Fourier, Espectroscopia de infravermelho por transformada de. I. Fernandez, Pablo Sebastian, 1983-. II. Universidade Estadual de Campinas. Instituto de Química. III. Título.

Informações para Biblioteca Digital

Título em outro idioma: Estudo da eletro-oxidação de glicerol em superfícies de platina e ouro modificadas por adátomos metálicos
Palavras-chave em inglês:
Glycerol
Electrooxidation
Metal adatoms
High performance liquid chromatography
Spectroscopy, Fourier transform infrared
Área de concentração: Físico-Química
Titulação: Mestre em Química na área de Físico-Química
Banca examinadora:
Pablo Sebastian Fernandez [Orientador]
Daniela Zanchet
Giuseppe Abíola Câmara da Silva
Data de defesa: 05-07-2018
Programa de Pós-Graduação: Química

BANCA EXAMINADORA

Prof. Dr. Pablo Sebastian Fernandez (Orientador)

Profa. Dra. Daniela Zanchet (IQ-UNICAMP)

Prof. Dr. Giuseppe Abíola Câmara da Silva (UFMS)

A Ata da defesa com as respectivas assinaturas dos membros encontra-se no processo de vida acadêmica do(a) aluno(a).

Este exemplar corresponde à redação final da Dissertação de Mestrado defendida pelo(a) aluno(a) **MATHEUS BATISTA CORDEIRO DE SOUZA**, aprovada pela Comissão Julgadora em 05 de julho de 2018.

Agradecimentos

Agradeço à minha família, por todo o apoio e suporte que me forneceram, durante toda a duração deste trabalho, e por virem de tão longe para assistir a defesa desta dissertação.

Aos amigos, tanto às amizades que fiz aqui em Campinas quanto aos que deixei em Recife. Muita gente me ajudou nessa jornada, seja no quesito profissional, me ajudando em experimentos ou explicando conceitos, ou no âmbito pessoal, me apoiando nos momentos de estresse, insegurança e afins. Sem eles, esse trabalho não teria sido realizado. Em especial, destaco os que estão comigo desde quando comecei a morar em Campinas: Laiane, Rosimeire, Raphael, Jessica e Marina.

Ao grupo de eletroquímica da Unicamp, do qual faço parte desde o início. Vários membros me ajudaram de uma forma ou de outra durante esse trabalho, com experimentos, debatendo ideias, entre outros. Em especial, agradeço aos que trabalham diretamente comigo: Rafael, pelos vários experimentos que fizemos em parceria, Victor, por todos os experimentos com monocristais, e ao Cleo, pelo seu enorme conhecimento e por toda a ajuda e paciência com o HPLC e coletor de amostras.

Agradeço à secretaria da CPG, Janaina, Isabela e Izabel, pela enorme paciência que tiveram para comigo, e por terem me ajudado durante os vários problemas com prazos e documentação que tive.

Ao prof. Jose Solla-Gullón, pesquisador visitante do grupo de eletroquímica da universidade de Alicante, que ajudou imensamente tanto a mim quanto ao nosso grupo de eletroquímica, mesmo durante uma curta temporada.

À FAEPEX, pela bolsa de estudos concedida durante o desenvolvimento desse trabalho.

Por último, mas não menos importante, ao prof. Pablo, que me orientou durante esse trabalho. Apesar das condições nas quais cheguei até ele, ele me aceitou como aluno, e me ensinou desde o básico da eletroquímica. Graças a essa oportunidade, e com muita paciência, conseguimos realizar esse trabalho. Durante esse tempo, a paciência dele aumentou em algumas ordens de grandeza.

Resumo

O objetivo geral dessa dissertação foi o estudo da eletro-oxidação de glicerol em meio alcalino em superfícies de ouro e platina, modificadas por adátomos metálicos. A modificação das superfícies foi feita por deposição sobrepotencial e adsorção irreversível, e os metais escolhidos para modificar os eletrodos foram cobre, chumbo e bismuto. Por meio de voltametria cíclica, foi concluído que o ouro foi desativado para a oxidação do glicerol após modificação com esses metais, observado pela redução na densidade de corrente registrada. A platina, por sua vez, foi desativada após modificação com cobre, ao passo que a modificação com bismuto promoveu a catálise, visto como um aumento na densidade de corrente. A adição de 10^{-5} M de óxido de bismuto ao eletrólito contendo glicerol em meio básico proporcionou o maior aumento em atividade e estabilidade do catalisador. Utilizando as técnicas de HPLC e FTIR, foi determinado que a adsorção do bismuto muda as vias de eletro-oxidação de glicerol da seguinte maneira: 1) inibe a formação de monóxido de carbono, um intermediário responsável pela desativação do catalisador, 2) promove a obtenção de ácido glicérico a partir do glicerol e 3) Reduz a oxidação total do glicerol à carbonato.

Abstract

The main goal of this dissertation was to understand the glycerol electrooxidation on platinum and gold surfaces in alkaline media, modified by deposition of metal adatoms. Surface modification was done using underpotential deposition and irreversible adsorption, and the metals chosen to modify the surfaces were copper, lead and bismuth. Using cyclic voltammetry, it was determined that gold was deactivated to glycerol oxidation after modification with the three metals, which generated a reduction in the current density. Platinum was also deactivated after modification with copper, however, bismuth promoted the catalysis, increasing the current densities. The optimum condition for this enhancement, was the addition of 10^{-5} M of bismuth oxide to the electrolyte containing glycerol. Using the HPLC and FTIR techniques, it was determined that the adsorption of bismuth modified the electrooxidation pathways as follows: 1) inhibits the formation of carbon monoxide on platinum, a poisoning intermediate responsible for catalyst deactivation, 2) promotes the conversion of glycerol into glyceric acid, and 3) hinders the glycerol complete oxidation towards carbonate.

Table of Contents

1. Introduction 9
   1.1. The importance of Glycerol 9
   1.2. Electrochemical valorization of glycerol 12
   1.3. Electrooxidation of glycerol on gold 19
   1.4. Electrooxidation of glycerol on platinum 21
   1.5. Electrochemical modification of noble metals 23
      1.5.1. Underpotential Deposition 23
      1.5.2. Irreversible adsorption 25
2. Objectives 27
3. Experimental 28
   3.1. Electrochemical system 28
   3.2. Electrode Modification 29
   3.3. High Performance Liquid Chromatography and on-line sample collection 32
   3.4. In-situ Fourier Transform Infrared Spectroscopy experiments 35
   3.5. Chemicals 35
4. Results and Discussion 37
   4.1. Surface Modification via Underpotential Deposition 37
   4.2. Irreversible adsorption of bismuth on platinum 39
   4.3. Glycerol electrooxidation on gold surfaces modified by metal adatoms 42
   4.4. Glycerol electrooxidation on platinum surfaces 43
      4.4.1. Copper-modified platinum 43
      4.4.2. Bismuth-modified platinum 44
         4.4.2.1. In-situ Fourier Transform Infrared Spectroscopy Analysis 50
         4.4.2.2. High-Performance Liquid Chromatography Analysis 53
         4.4.2.3. Electrochemical, chromatographic and spectroscopic results 55
5. Conclusions 60
6. Perspectives 61
7. References 62
8. Appendix 70
   8.1. Determination of theoretical cell voltages 70
   8.2. Supporting information 72

1. Introduction

1.1. The importance of Glycerol

The combination of increasing global energy demand and depletion of fossil fuel reserves has inspired researches across various fields to look for alternative, renewable energy sources. The demand for these renewable sources has seen a constant increase throughout the years, in addition to the continuous advances in both technology and research on this field[1]. One of the several renewable energy sources is the biomass. Biomass can be used as an energy source either in its natural form, or refined into gaseous or liquid biofuels, such as syngas, biogas, bio-ethanol and biodiesel[2]. Biodiesel, in particular, has been proposed as a substitute for conventional diesel oil, and has attracted more attention in the recent years.

Biodiesel is produced from the transesterification of vegetable oils and animal or waste fats. This process consists of breaking the fatty acids into smaller molecules, generating fat-derived esters (either methyl or ethyl), the biodiesel, and the glycerol (GOH) backbone, the main by-product, with a 10wt% yield[3] (scheme 1).

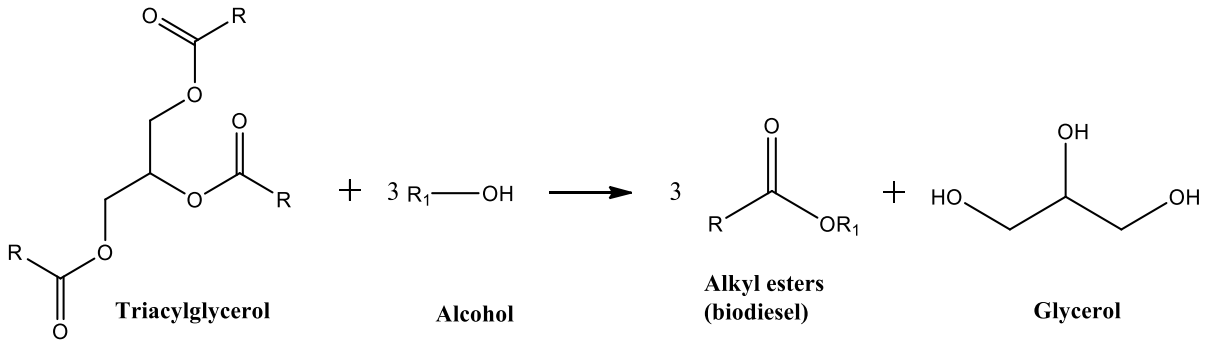

Scheme 1: Transesterification reaction of vegetable oils and fats, resulting in alkyl esters (biodiesel) and glycerol.

The global production and demand for biodiesel has been continuously increasing throughout the years[1], and with it the availability of GOH. This increasing demand caused a shift on its market, as the previous main supplier was the oleochemical industry, and now the main source is the biodiesel industry[3]. This surplus

of crude GOH, from biodiesel production, has caused a significant price drop on its value, negatively impacting the biodiesel industry, which already suffers with high production costs[4]. GOH is mainly used as an additive in food production and as a building block in the pharmaceutical and cosmetics industries, although the use of crude GOH is avoided, as its contaminants (methanol, salts and free fatty acids) cause damage to the piping and storage systems[3]. Refining this crude GOH involves high-temperature vacuum distillation, which is only cost-efficient in large-scale operations[3]. Although deemed unsuitable for most industrial applications and electrochemical studies, there are reports citing its use as anode feedstock in alkaline fuel cells[5–7].

The combination of large availability and price drop has led many researchers to investigate the chemical valorization of GOH[2–4,8–10], involving the synthesis of several value-added products (figure 1)[2] and its use as an energy source in fuel cells[9,11].

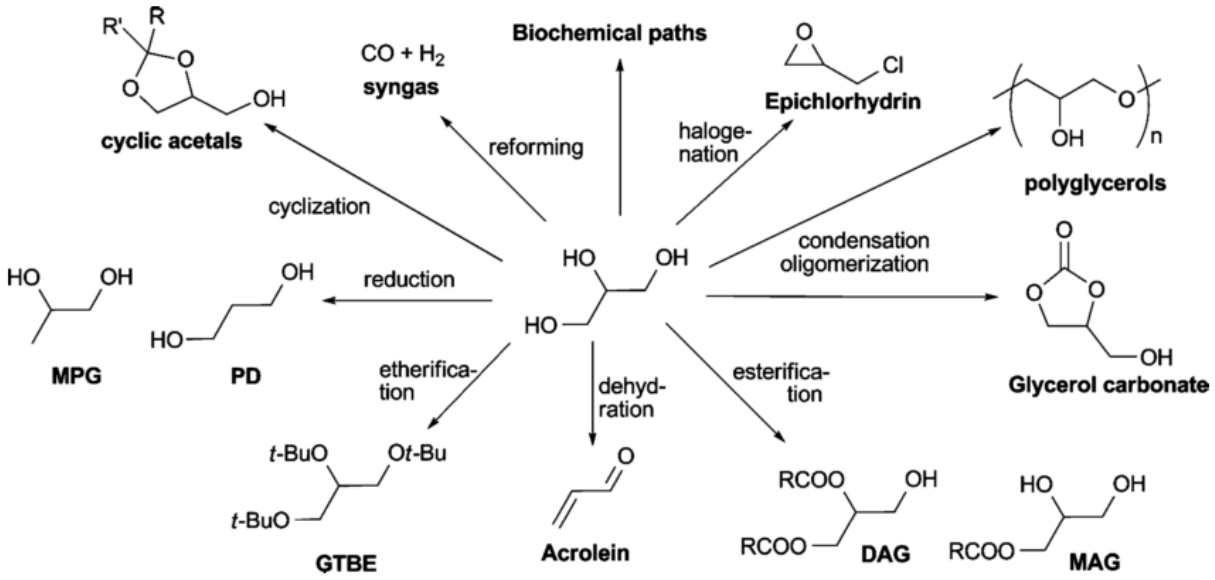

Figure 1: Some possible chemical valorization routes for glycerol. Reproduced with permission from ref. [2].

Glycerol, or propane-1,2,3-triol, is a polyol with two primary hydroxyl groups and a secondary one. It is a molecule with a high theoretical energy density (5.0 $kWh.kg^{-1}$), since its complete oxidation to CO_2 involves the exchange of 14 electrons[11].

In addition to the valorization routes shown in scheme 2, GOH can be oxidized into several C_3, C_2 and C_1 products (figure 2), often involving several parallel reactions, thus requiring highly specific catalysts in order to control the product selectivity, which also depends on the solution composition, pH, temperature, etc.

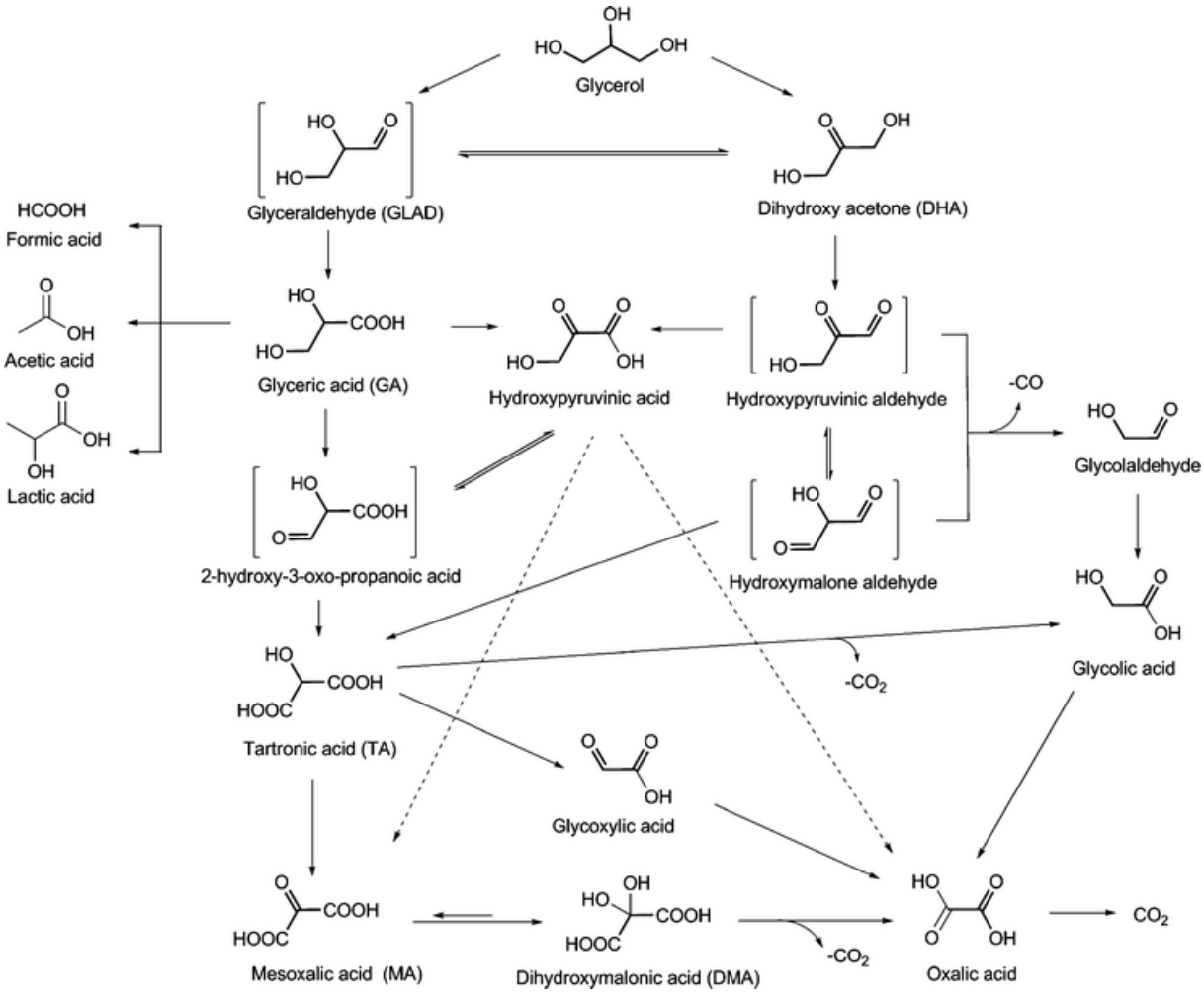

Figure 2: Possible products obtained from glycerol oxidation. Reproduced with permission from ref. [2].

The catalytic conversion of GOH has not been commercially applied until now[2]. However, there have been several works reporting the selective oxidation of GOH to value-added products, mostly via conventional heterogeneous catalysis methods, but also by means of electrochemical oxidation. GOH has been selectively oxidized to dihydroxyacetone[12–15], lactic acid[16], glyceric acid[15,17,18], among others[2,19,20].

Table 1 shows the price of some C_3 oxidation products of GOH, known to be generated via electrochemical conversion[11,21].

Table 1: Price of some C_3 oxidation products of GOH, generated via electrochemical oxidation. In some cases, the price of the cheapest salt is presented, as the acids were not found on the online catalogue. Adapted from ref. [8].

Chemical compound	Price (US$.g^{-1})
Glycerol	0.33
Sodium mesoxalate monohydrate (purity ≥ 98%)	5.95
Tartronic acid (purity ≥ 97%)	6.53
Glyceraldehyde (purity ≥ 90%)	86.50
Dihydroxyacetone	1389.60
Glyceric acid sodium salt (purity ≥ 95%)	3812.00
Hydroxypyruvic acid (purity ≥ 95%)	18,740.00

1.2. Electrochemical valorization of glycerol

The glycerol electrooxidation reaction (GEOR), is one of the many options to GOH valorization. This process was first employed during the 1980s[22,23] using gold and platinum electrodes as catalysts. After a significant time with no innovations on this field, as no major studies were conducted on it, the interest on the subject flourished in the early 2010s, when two major studies were published. In the first one, GOH was employed as a fuel source in direct alkaline alcohol fuel cells[11], while in the other the GEOR was used as model reaction in the development of a technique which combined cyclic voltammetry with *on-line* sample collection, for later HPLC analysis (named as *on-line* HPLC by the authors)[24]. The results obtained in those works encourage many other groups around the world to study the GEOR.

The conversion of GOH using electrochemical reactors offers many advantages over conventional heterogeneous reactors. With electrochemical reactors, this process can be performed at room temperature and ambient pressure, as no thermal activation is required. Control of the electrode potential, electrolyte pH, GOH concentration and flow rate (when a flow cell is used) are other factors that, when combined, allow precise control of the reaction selectivity[9].

On the other hand, electrochemical systems are more complex than conventional heterogeneous processes, because the potential distribution across the reactor is influenced by the electrode material and its form, reactor design, mass transport of reactants and products, hydrodynamics and current distribution[25]. The potential distribution has a significant impact on selectivity and process scale up, thus an electrochemical process requires considerably more work than the heterogeneous counterpart in order to reach the level of industrial application.

In addition to the aforementioned parameters, the use of shape-controlled nanoparticles as electrocatalysts[26–29] allows tuning the catalyst surface to specific crystallographic orientations, since site-preference is observed during the electrooxidation of several organic molecules[13,30–32]. The surface of electrocatalysts can be easily modified via electrochemical methods[33,34], using either the underpotential deposition or irreversible adsorption techniques, which will be explained in a later section.

Another advantage of the electrochemical oxidation of alcohols is that it can be coupled with H_2 generation in an electrolyzer[8–10]. Figure 3 shows the working principle of a GOH-based alkaline electrolysis cell. The application of an external electric field promotes the oxidation of GOH at the anode, producing value-added oxidation products, while releasing water and electrons. These electrons are forced towards the cathode side through an external circuit, where water is reduced to H_2. The hydroxyl ions generated in the process flow across a permeable membrane towards the anode.

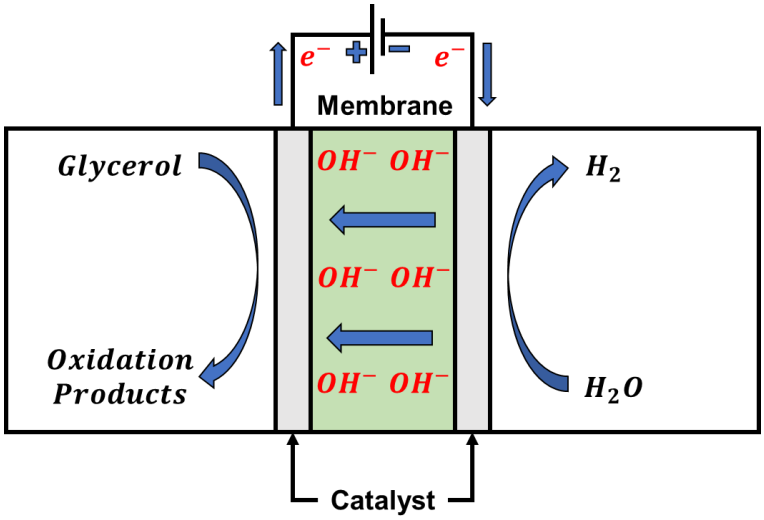

Figure 3: General scheme of a GOH-based electrolysis cell. GOH is oxidized at the anode (left side), releasing its value-added products, water and electrons. The electrons are forced to the cathode (right side) through an external circuit, where water is reduced to H_2, releasing hydroxyl ions, which flow towards the anode side through a permeable membrane.

The GOH at the anode side can be either completely oxidized, generating CO_3^{2-} and releasing 14 electrons, maximizing the H_2 production, or partially oxidized, where the reduced gaseous hydrogen production rate is compensated by the generation of value-added products on the anode, instead of carbonate[8–10]. The electrochemical reactions occurring on the electrolysis cell for the complete oxidation of GOH are:

$$CH_2OH - CHOH - CH_2OH + 20\,OH^- \rightarrow 3CO_3^{2-} + 14H_2O + 14e^- \quad (1)$$

$$2H_2O + 2e^- \rightarrow H_2 + 2OH^- \quad (2)$$

$$CH_2OH - CHOH - CH_2OH + 6OH^- \rightarrow 3CO_3^{2-} + 7H_2 \quad (3)$$

where reactions (1) and (2) occur on the anode and cathode, respectively, and (3) is the overall reaction. The theoretical cell voltage (E°_{cell}), can be calculated using $E^\circ_{cell} = -\Delta G_r^\circ / nF$ [35], where ΔG_r° is the standard Gibbs free energy of the reaction, n the number of electrons involved in the electrochemical reaction, and F the Faraday constant. Using standard thermodynamic data[36,37], the cell voltage for this cell is $E^\circ_{EC,GOH} = +0.062\ V$, where EC stands for electrolysis cell. For a water-based electrolysis cell

(water splitting), this value is $E^{\circ}_{EC,H_2O} = -1.229\ V$[9,10]. The cell voltage in an electrolyzer represents the minimum voltage that needs to be applied in order for electrolysis to occur, i. e. it is an energy barrier that must be surpassed. This thermodynamic data shows that a GOH-fed electrolyzer requires significantly less energy to operate than conventional water splitting devices, also valid for other alcohol-based electrolyzers, however several limitations lead to an increase in the potential difference between the electrodes, hence limiting their applicability[10]. It is interesting to note that $E^{\circ}_{EC,GOH} > 0$, indicating that the reaction occurs spontaneously. However, due to this very low thermodynamic potential difference and the slow kinetics of GOH oxidation, an external energy supply is necessary in order for the electrolysis cell to operate at an appreciable rate.

Another possibility for the electrochemical valorization of GOH consists on its use as an energy source in fuel cells[9–11]. A fuel cell is a device similar to the electrolyzer (figure 3), however no external potential needs to be applied to the device, i. e. the reaction occurs spontaneously, with generation of an electrical current (energy), that can be harnessed to power other devices. Figure 4 shows a general scheme of a GOH-fed fuel cell. Similar to the electrolyzer, GOH is fed on the anode side of the device, where it oxidizes, generating value-added products and releasing electrons. The electrons travel through the external circuit producing electric work, and later flow towards the cathode. In the cathode, oxygen is reduced into hydroxyl ions, which flow to the anode side through a permeable membrane[9].

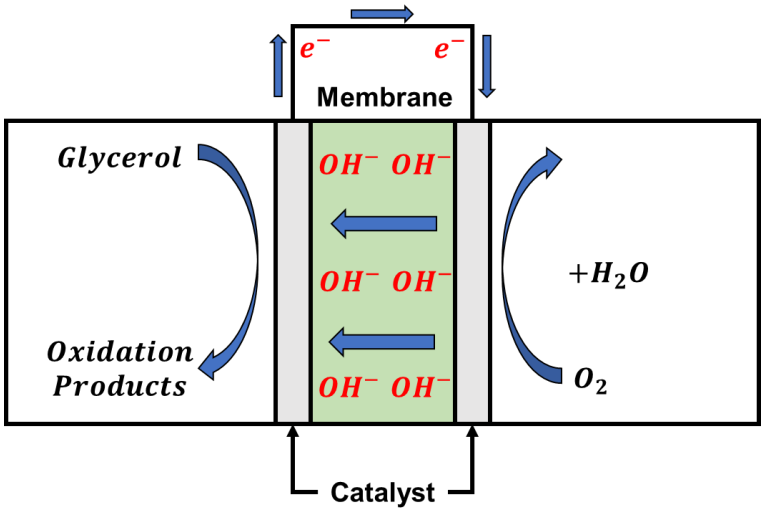

Figure 4: General scheme of a GOH-fed fuel cell. GOH is oxidized at the anode (left side), releasing its value-added products, water and electrons. The electrons travel outside the cell to perform electrical work, powering other devices. In the cathode, they reduce oxygen into hydroxyl ions. The hydroxyl ions flow towards the anode side through a permeable membrane.

The electrochemical reactions on the GOH-based alkaline fuel cell are as follows:

$$CH_2OH - CHOH - CH_2OH + 20\ OH^- \rightarrow 3CO_3^{2-} + 14H_2O + 14e^- \quad (1)$$

$$^1/_2\ O_2 + H_2O + 2e^- \rightarrow 2\ OH^- \quad (4)$$

$$CH_2OH - CHOH - CH_2OH + {}^7/_2\ O_2 + 6\ OH^- \rightarrow 3CO_3^{2-} + 7H_2O \quad (5)$$

Reaction (1) is the same as in the electrolyzer, while on the cathode side gaseous oxygen is reduced according to reaction (4), and (5) is the overall reaction. The calculated cell potential for this device is $\mathrm{E}^{\circ}_{\mathrm{FC,GOH}} = +1.291\ V$, where FC stands for fuel cell. In comparison, the calculated cell potential for a hydrogen/oxygen alkaline fuel cell is $\mathrm{E}^{\circ}_{\mathrm{FC},\mathrm{H_2}/O_2} = +1.229\ V$ [38]. Instead of representing an energy barrier, like in the electrolyzer, the cell potential here represents the maximum power output (voltage) that can be obtained from such a device[10,38]. The typical cell voltage (useful) for high performance H_2/O_2 fuel cells is between 0.6 – 0.7 V[9,10,38]. This difference from the theoretical voltage is caused by losses during cell operation, caused by ohmic/internal

loss (internal resistance, mainly from the membrane, materials used, cell design), kinetics (activation loss, slow redox kinetics of oxygen, requiring high overpotentials) and mass transport/concentration losses (when the reactants cannot be delivered fast enough to the catalyst sites, and if there is anything preventing the reactant flow)[10,38]. As for electrolyzers, thermodynamic data supports the use of GOH and other alcohols as an energy source for fuel cells[9–11,26], however their applicability still has several constraints[10].

To the best of our knowledge, no commercial GOH-powered fuel cell or electrolyzer is available on the market, and all known devices are in the prototype phase[8]. In both devices, the anode side is the same (fed by GOH), therefore, as was stated before, it is the cathode side that determines if the reaction is spontaneous (fuel cell) or not (electrolyzer). This spontaneity is controlled by thermodynamic considerations, mainly the standard cell potential (E°). Figure 5 provides a general overview to the significance of this parameter on these devices, where the theoretical current-potential curves for hydrogen, oxygen and GOH redox processes are represented according to the Butler-Volmer kinetics[35].

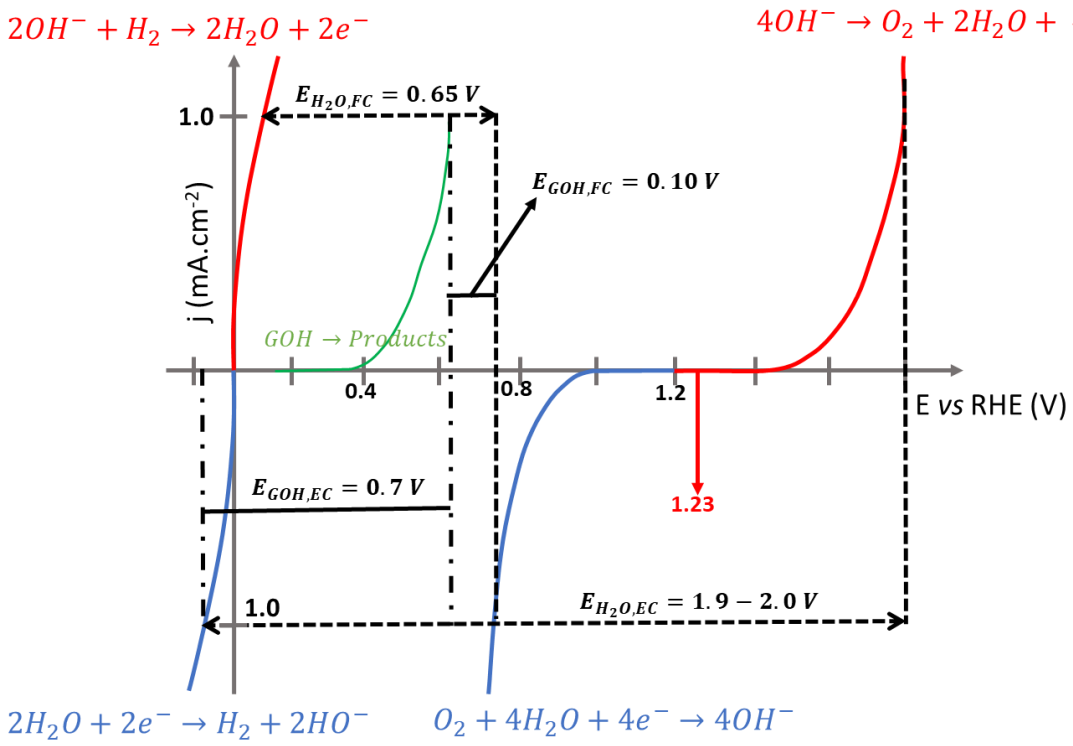

Figure 5: Comparison of the theoretical current-potential curves for the redox processes of water, hydrogen and GOH, following the Butler-Volmer law. $E_{H_2O,FC}$ and $E_{H_2O,EC}$ are the cell voltages for water-based fuel cells and electrolyzers, respectively, while $E_{GOH,FC}$ and $E_{GOH,EC}$ represent the same but for GOH-fed fuel cells and electrolyzers, respectively. $E° = 1.23\ V\ vs\ RHE$ is the H_2O/O_2 reversible reaction potential. Adapted from refs. [9,10].

In figure 5, the red curves represent the oxidation of both H_2 and H_2O, while the blue curves account for their oxidation, and the green curve represents the observed GOH oxidation. The kinetics of O_2 oxidation-reduction are quite slow, therefore high overpotentials are necessary (1.8 – 2.0 V) to produce H_2 in significant amounts in a water splitting electrolyzer. Feeding GOH or other alcohols may significantly reduce this overpotential[9,10]. In electrolyzers, catalysts who provide high current densities with minimal overpotential are desired, in addition to the selective oxidation of GOH. Whereas in a fuel cell, catalysts capable of oxidizing GOH to carbonate at low potentials with high currents are desired.

1.3. Electrooxidation of glycerol on gold

Several mechanisms have been proposed for the GEOR on Au electrodes in alkaline media[11,21,22,24,39–41]. Nowadays, the most widely accepted mechanism is the one proposed by Kwon et. al.[21,24], derived from a combination of electrochemical methods and HPLC.

In this mechanism, GOH initially undergoes a primary alcohol oxidation where it is oxidized in a two-electron transfer step to glyceraldehyde, starting at 0.8 V, followed by a second two-electron transfer step to glyceric acid. However, glyceraldehyde consists of an unstable intermediate on gold, both due to the high effective overpotential on the electrode, a consequence of its delayed surface oxidation (around 1.3 V), and to its tendency to oxidize when in alkaline media[42], therefore glyceric acid is apparently directly produced from GOH via glyceraldehyde. Glyceric acid is further oxidized by a two-electron transfer step, at 0.85 V, resulting in C-C bond breaking into glycolic acid and formic acid. Au has a high conversion rate of glyceric acid into glycolic acid, and formic acid, which was ascribed to the high effective overpotential applied on the electrode. The mechanism proposed by Kwon and co-workers [21] is shown in scheme 3.

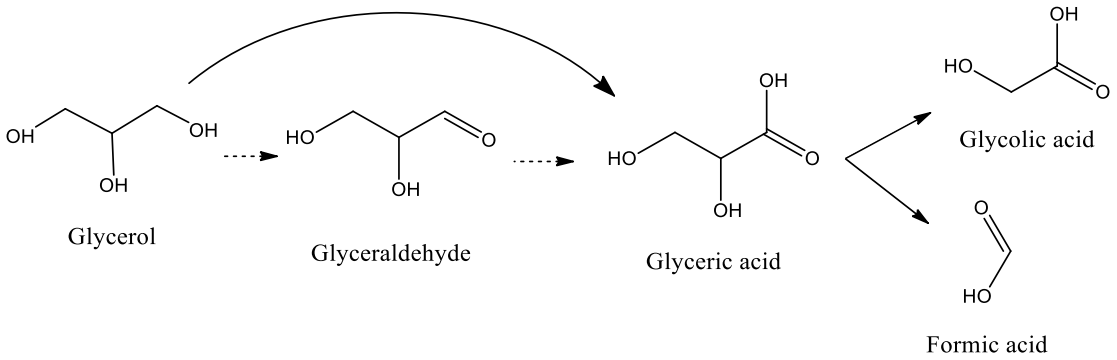

Scheme 3: Reaction scheme for the GEOR on Au in alkaline media, proposed by Kwon and co-workers [21], from electrochemical and HPLC results. Full arrows indicate the observed reactions, the dashed arrows indicate the proposed reaction pathway.

The electrolyte pH, plays an important role in the GEOR on Au. Gold is inactive to the GEOR in acidic media[21,22], and only slightly active in neutral media[21]. In order for the GEOR to occur on Au, the pH has to be high in order to maintain the catalyst surface covered with adsorbed hydroxyl molecules, forming the Au(OH) species on the electrode surface[39,43]:

$$Au + OH^- \rightleftharpoons Au(OH)_{ads}^{\delta-} + \lambda e^- \quad (6)$$

where $\mathrm{Au(OH)_{ads}^{\delta-}}$ is the catalyst active site with surface bound to hydroxyl species, and λ is the voltage dependent partial charge transfer[39,43]. This species is capable of combining with either GOH or the glycerolate anion, originated from GOH deprotonation[41,43], into glyceraldehyde at the electrode surface. Reaction (7) shows the GOH deprotonation, while reactions (8) and (9) are the GOH and glycerolate oxidation, respectively.

$$CH_2OH - CHOH - CH_2OH \rightleftharpoons CH_2OH - CHOH - CH_2O^- + H_\alpha^+ \quad (7)$$

$$C_3H_8O_3 + Au(OH)_{ads}^{\delta-} + OH^- \rightleftharpoons Au + C_3H_6O_3 + 2H_2O + (1+\delta)e^- \quad (8)$$

$$C_3H_7O_3^- + Au(OH)_{ads}^{\delta-} \rightleftharpoons Au + C_3H_6O_3 + H_2O + (1+\delta)e^- \quad (9)$$

Reaction (7) shows a further role of the alkaline media as a catalyst. This scenario occurs when the solution pH approaches the pKa of GOH, 14.15[43]. This is a solution-phase reaction, where the electrode plays no role[41,43].

Since the glycerolate anion is more reactive than GOH[41], reaction (9) can occur at lower overpotentials than reaction (8), accounting for the role of base-catalysis of the GEOR on gold[43]. The GOH and glycerolate molecules have a preferential adsorption configuration by adsorbing the CH/CH_2 group at the $\mathrm{Au(OH)_{ads}^{\delta-}}$ site, due to their weaker hydration[43,44], which facilitates the dehydrogenation into glyceraldehyde. The overall reaction is obtained when reaction (6) is combined with reactions (8) and (9), as follows:

$$C_3H_8O_3 + 2OH^- \rightleftharpoons C_3H_6O_3 + 2H_2O + 2e^- \quad (10)$$

$$C_3H_7O_3^- + OH^- \rightleftharpoons C_3H_6O_3 + H_2O + 2e^- \quad (11)$$

One of those reactions, either the dehydrogenation of GOH or glycerolate anion, is thought to be the rate-determining step of the GEOR on gold surfaces[43].

Despite being often used as an electrocatalyst in the GEOR, more active than Pt in alkaline media at higher potentials[22,24,41], few studies exist were the Au electrode is modified by metal adatoms[19]. On the other hand, Pt electrodes have been extensively modified via adatom deposition[13,30–32,45], and their impact on catalyst activity and selectivity has been established. With this in mind, we decided to modify polycrystalline Au electrodes with metal adatoms to verify their influence on the activity and selectivity of the GEOR.

1.4. Electrooxidation of glycerol on platinum

The GEOR on Pt electrodes, unlike Au, occurs regardless of electrolyte pH, however the current densities shown in alkaline media are significantly higher[21,22] than what is observed in neutral or acidic conditions. Pt has a lower onset potential than Au, it begins to oxidize GOH at 0.4 V, whereas oxidation on Au only begins at 0.8 V[21]. It was proposed that the GEOR is strongly promoted by hydroxyl anions, both in Au and Pt catalysts[21]. The GEOR on Pt electrodes has been more investigated in acidic media, where the GOH complete oxidation to CO_2 has been detected[46], and it is already known that the primary hydroxyl groups are more easily oxidized than the secondary one, although both groups contribute to the CO_2 production[47]. The effect of electrode structure has also been investigated[48–50], using low-index Pt single crystals [(111), (110) and (100)]. It has been found that the GEOR is highly sensitive to the electrode structure[50], and that both CO and GOH bind more strongly on disturbed than on well-ordered surfaces[48]. In order to oxidize GOH in acidic media without poisoning the electrode, moderately high potentials are required, in order to oxidize the adsorbed CO into CO_2[49]. The Pt – CO bond breaking has been considered as the rate-determining step to the GEOR in acidic media[48]. To the best of our knowledge, no such detailed investigation of the GEOR in alkaline media has been performed using Pt single-crystal electrodes, even though the current densities are significantly higher. In alkaline media, a study[51] with a (111) Pt single crystal has hypothesized that electrode deactivation is due to strongly adsorbed acyl species, formed during the GEOR, and not CO poisoning.

The most widely accepted reaction scheme proposed for the GEOR on a Pt electrode in alkaline media is the one proposed by Kwon et. al.[21,24], derived from electrochemical and HPLC analysis, shown below.

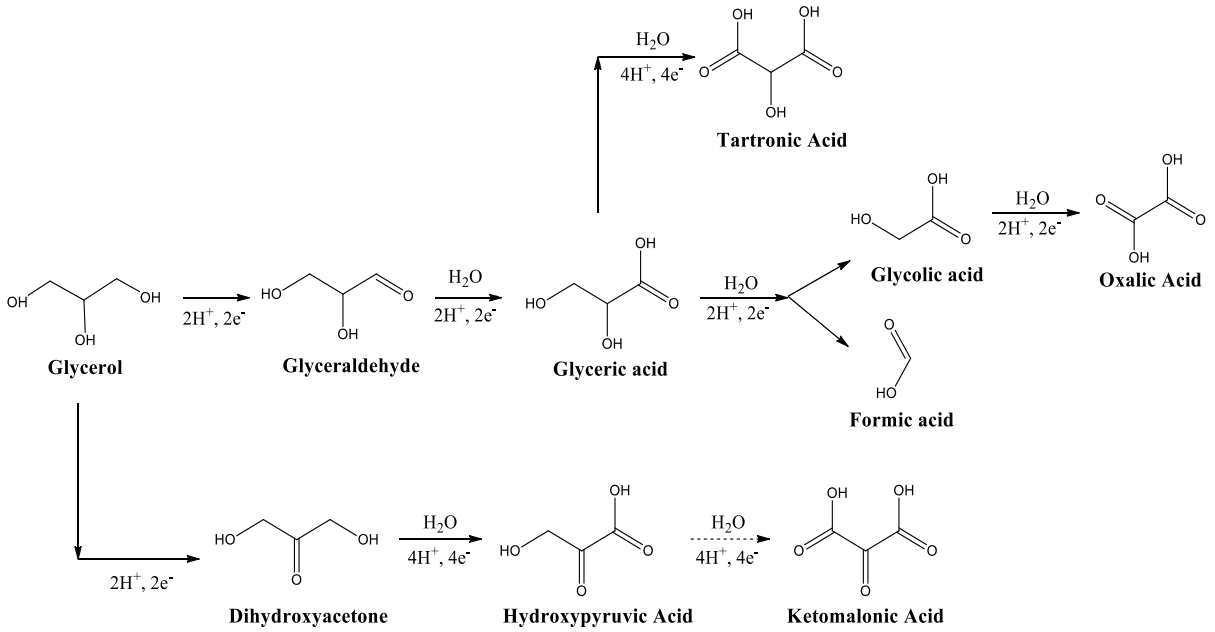

Scheme 4: Reaction mechanism for the GEOR on Pt in alkaline media, proposed by Kwon and co-workers [21], from electrochemical and HPLC results. Full arrows indicate the observed reactions, the dashed arrows indicate the proposed reaction pathway.

The main difference between this mechanism and the one shown in scheme 3, for the GEOR on an Au electrode, is that on Pt the GOH can undergo either a primary or secondary alcohol oxidation pathway. In the path of primary oxidation pathway, GOH is initially oxidized to glyceraldehyde, now a stable product, through a two-electron transfer step, and a subsequent two-electron transfer step into glyceric acid. Glyceric acid is further oxidized by cleavage of a C-C bond via another two-electron transfer step, resulting in formic acid and glycolic acid. This step occurs at a higher rate on the Au electrode than in Pt and was attributed to the delayed surface oxidation of the Au electrode. Glycolic and glyceric acid can be further oxidized into oxalic and tartronic acid, respectively. In the pathway of secondary alcohol oxidation, GOH is

oxidized into dihydroxyacetone by a two-electron transfer step, and further oxidized into hydroxypyruvic and ketomalonic acid.

Modification of Pt with deposition of metal adatoms has been extensively described in the literature[13,30–32,45]. In particular, bismuth is known to enhance the catalytic activity of Pt towards the oxidation of several organics, such as formic acid[30,32], methanol[30] and GOH, both in acidic[13] and alkaline[52] media. With this in mind, we decided to investigate the effects of adatom modification on Pt to the GEOR in alkaline media, since previous studies were mainly focused on acidic media[13,45,53]. Modification with Bi was of particular interest, since in acidic media it was found to selectively oxidize GOH to dihydroxyacetone[13], one of the high value-added GOH oxidation products (Table 1).

1.5. Electrochemical modification of noble metals

In this work, we modified Pt and Au electrodes using adatoms. Below, we introduce and explain the most relevant characteristics of the approaches used here, i.e., the under potential deposition and irreversible adsorption.

1.5.1. Underpotential Deposition

When a metal is electrodeposited on a foreign substrate, an apparent violation Nernst's law is observed[54]. Metal deposition takes place at potentials lower than predicted by the Nernst equilibrium potential, however the opposite happens in the case of underpotential deposition (UPD)[33,34]. This process can be better visualized using the concept of overpotential (overvoltage), represented by the letter η, defined as:

$$\eta = E - E_{M_{(bulk)}/M_{aq}^{z+}}$$

where E is the actual potential on the electrode, and $E_{M_{(bulk)}/M_{aq}^{z+}}$ is the Nernst equilibrium potential of the following reaction:

$$M_{(bulk)} \rightleftarrows M_{(aq)}^{z+} + ze^{-}$$

where $M_{(bulk)}$ stands for the metallic material and $M_{(aq)}^{z+}$ represents the corresponding metallic ion in aqueous solution and with charge z. Controlling the potential on the electrode dictates the direction of this reaction. When $E < E_{M_{(bulk)}/M_{aq}^{z+}}$, the metal ions reduce and deposit on the electrode surface of the same origin, i.e., there is a 3D growth of the bulk metal phase due to cathodic deposition, and in this scenario $\eta < 0$. This type of deposition, with a negative overpotential, is called overpotential deposition (OPD), and is associated with formation of 3D metal phases[33]. When $E > E_{M_{(bulk)}/M_{aq}^{z+}}$, the bulk metal phase dissolves anodically and $\eta > 0$.

In the case of a M phase formation on a foreign substrate (S), the overall reaction on S/M^{z+} pair is:

$$M_{(on\ S)} \rightleftharpoons M_{aq}^{z+} + ze^{-}$$

where $M_{(on\,S)}$ denotes the metal atom deposited on the foreign substrate S. The electrode potential determines the direction of this reaction, however the Nernst equilibrium potential on the overpotential equation is with respect to the substrate S, as follows:

$$\eta' = E - E_{(M\ on\ S)/M_{aq}^{z+}}$$

The term $E_{(M\ on\ S)/M_{aq}^{z+}}$ represents the Nernst equilibrium potential of the metal ion M^{z+} reducing and depositing on the foreign substrate S. Under certain conditions[33,34], a 2D metal phase is stable on this substrate S, and in this scenario, $E_{(M\ on\ S)/M_{aq}^{z+}} > E_{M_{(bulk)}/M_{aq}^{z+}}$, that is, the metal ion can be deposited in a potential range where only its cationic form is found without the presence of S. This potential range is:

$$\Delta E = E_{(M\ on\ S)/M_{aq}^{z+}} - E_{M_{(bulk)}/M_{aq}^{z+}}$$

This ΔE can be better visualized in figure 6 below. In this potential interval, the metal ion is reduced on top of substrate S, forming a 2D phase, in a region where $E > E_{M_{(bulk)}/M_{aq}^{z+}}$, which corresponds to $\eta > 0$. This deposition of a 2D metal phase on a foreign substrate, with a positive overvoltage, is named *under*potential deposition, because the term *over*potential was already coined for metal deposition in $\eta < 0$, resulting in this contradictory denomination[34].

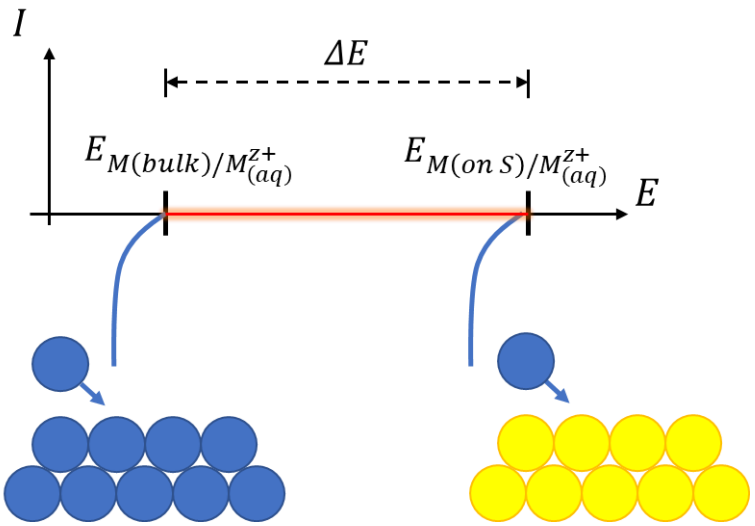

Figure 6: Current-potential diagram showing the Nernst equilibrium potential for deposition of $M_{(aq)}^{z+}$ on $M_{(bulk)}$ and on a foreign substrate S (blue and yellow circles, respectively). ΔE, the difference between these two values, is the potential interval (red line) in which UPD takes place.

The UPD is a reversible process, and the adatoms obtained by this method are more strongly bound to the foreign surface than to their bulk counterparts, which can be used to determine the binding energy of the substrate and adsorbate[54]. For UPD to occur, there must be an equilibrium between the interphase and the solution containing the metal ions, and it can only form, at most, two layers on the foreign substrate[33]. This allows precise surface modification; however, the coverage is a function of both applied potential and solution composition[55].

1.5.2. Irreversible adsorption

Irreversible adsorption occurs when the metal adatoms, in their cationic form, undergo spontaneous reduction and subsequent adsorption on the electrode surface, without an applied potential (open circuit condition). Such scenario occurs by immersion of the electrode in a solution containing a soluble salt of the desired element. Different to UPD, in this case there is no equilibrium between the adsorbed species on the electrode surface and the cations in the solution[55]. This situation

constitutes a significant advantage over the UPD, since electrode coverage can be varied independently of electrode potential

It is important to note, however, that the adsorption of these adatoms is not completely irreversible. Applying a sufficiently high potential on the electrode will cause the adatoms to leave the electrode surface, as seen in the case of Bi[56] and Pb[57] adsorption on Pt. To the best of our knowledge, the mechanism of this process has not been completely elucidated, and several propositions have been made[55].

Even if several aspects of the Bi deposition on Pt have not been elucidated, the promotion of some reactions for the adatom motivate researchers to investigate fundamental aspects of this system that are enumerated as follow. Bi adsorbs irreversibly on Pt by immersion of the electrode on an acidic solution of a Bi salt at open circuit condition[56]. This deposition takes place even at an oxidized Pt surface, and the UPD of Bi on Pt coincides with the reduction of the surface oxides[58]. Bi deposits irreversibly on Pt in its metallic state, covering 1/3 of a monolayer on the electrode, while the other 2/3 is covered by adsorbed OH^- species[59]. Besides a physical site blocking effect, Bi is capable of altering the electronic properties of Pt, by lowering the work function of Pt(111)[60] and reducing the potential of zero charge (pzc*)* for both Pt(111) and Pt(100)[59,61,62]. This reduction of the pzc causes the Pt atoms neighboring the adsorbed Bi to be positively charged in respect to the unmodified Pt surface, resulting in an enhanced anion adsorption and, consequently, reduced H adsorption. Therefore, two distinct sites are present for OH adsorption, the Pt sites which are electronically influenced by Bi, and the unmodified Pt sites.

2. Objectives

The primary objective of this work is to understand the impact of electrode modification on the GEOR in alkaline media on gold and platinum surfaces. We will modify the electrodes with a full or partial adlayer of metal atoms (Cu, Bi and Pb), and observe the impact on catalyst activity using cyclic voltammetry. For the catalysts that show a higher activity after modification, the oxidation products will be identified and quantified using a combination of *in-situ* FTIR and HPLC with *on-line* sample collection.

Ultimately, we aim to understand the relationship between catalyst structure, activity and reaction pathways for the GEOR.

3. Experimental

3.1. Electrochemical system

A standard three-electrode cell was employed during the electrochemical measurements (figure 6). The working electrodes were polycrystalline platinum (Pt_{poly}) and gold (Au_{poly}), consisting of the metal wire (Alfa Aesar) with a spherical end. The counter electrodes used in those experiments were either platinum and gold foils (Alfa Aesar), when the Pt_{poly} and Au_{poly} electrodes were used as WE, respectively. The reference electrode was a reversible hydrogen electrode (RHE). All potentials in this text are referred to the RHE. The potential of the working electrode was measured always against the RHE and controlled by a potentiostat/galvanostat Autolab PGSTAT101, Methrom® (figure 7).

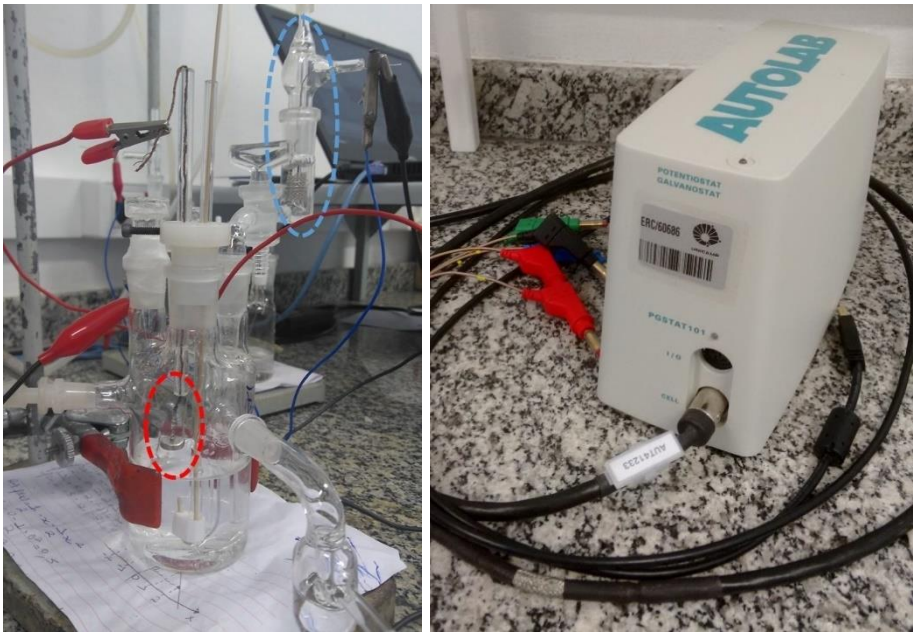

Figure 7: (left) electrochemical cell used on the electrochemical measurements, highlighting the working (red) and reference (blue) electrodes; (right) the potentiostat/galvanostat used to control the cell.

All glassware was cleaned by immersion in an alkaline $KMnO_4$ solution overnight. Afterwards, they were rinsed with ultrapure water and a solution of H_2SO_4 + H_2O_2.. Lastly, the glassware was again rinsed with deionized water, and boiled in ultrapure water for 10 minutes, three times. Before any electrochemical measurements, a voltammogram of the electrode is recorded in the blank electrolyte, commonly called the "blank voltammogram" of the electrode. This blank is necessary to confirm the cleanliness of the electrochemical system, i.e., the electrodes and the electrolytes. The blank voltammogram of Pt_{poly} and Au_{poly} in acidic and alkaline media is shown in figure 8. The electrochemical measurements were only initiated if the registered blank corresponds to the ones shown below.

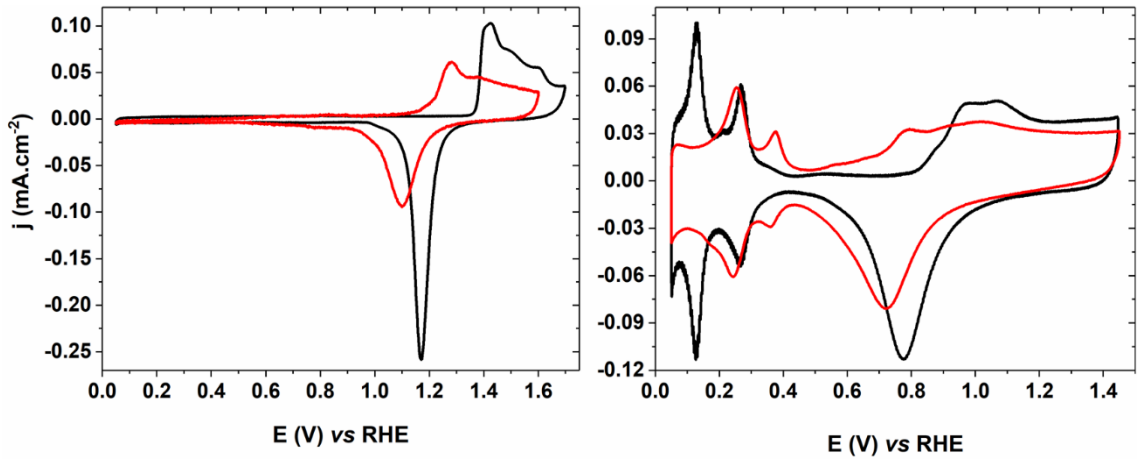

Figure 8: Blank voltammograms for Au_{poly} (left) and Pt_{poly} (right) in 0.5 M H_2SO_4 (black) and 0.1 M NaOH (red). Scan rate was 10 $mV.s^{-1}$.

3.2. Electrode Modification

Electrode surface modification was performed using both the irreversible adsorption and UPD methods. Irreversible adsorption of Bi[56] on Pt_{poly} was performed by immersion of the working electrode in an acidic bismuth solution, with 0.5 M H_2SO_4 and Bi_2O_3 concentrations ranging from 10^{-3} to 10^{-5} M. The electrode was immersed at open circuit (no potential control) for a set amount of time, rinsed with ultrapure water and transferred to an electrochemical cell with a 0.1 M NaOH electrolyte, and a blank voltammogram was recorded in the potential window from 0.05 to 0.45 V to determine

the electrode coverage (θ). Due to the shape of our electrode, a Pt wire with a spherical end, the amount of the electrode that was immersed into the acidic Bi solution and into the electrochemical cell varies within an experimental error, therefore reproducing a specific value of θ is not guaranteed even if the Bi^{3+} concentration and the immersion time are fixed.

The electrode was immersed in the electrolyte solution polarized at the upper potential, followed by negative scan to the lower potential. The coverage was calculated from the decrease in the hydrogen desorption peaks, after a stable voltammogram was obtained (figure 9), using the equation below:

$$\theta = 1 - \frac{Q_{H,modified}}{Q_{H,unmodified}}$$

where $Q_{H,modified}$ is the charge associated with the hydrogen desorption in a modified Pt electrode, and $Q_{H,unmodified}$ is the charge associated with hydrogen desorption in a clean Pt electrode. This charge is obtained by integrating the faradaic portion of the positive-going scan of the blank voltammogram, the area above the red dashed line in figure 8, between 0.05 and 0.45 V, and dividing by the scan rate. The dashed red area in figure 8 represents the amount of charge lost after electrode modification, i. e. it represents $Q_{H,unmodified} - Q_{H,modified}$.

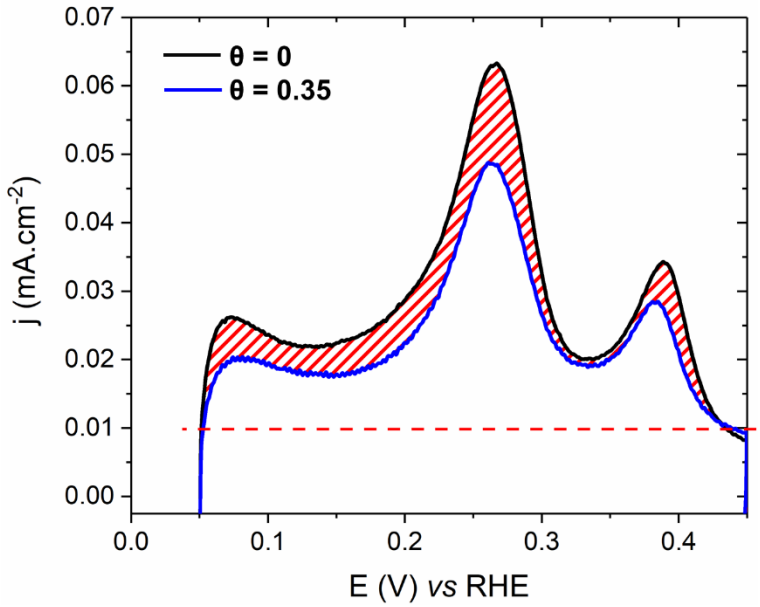

Figure 9: Calculation scheme of the electrode coverage determination. The hydrogen desorption charge for a clean Pt_{poly} electrode (black) and partially covered (blue) is obtained by integrating above the red dashed line. The dashed area between the curves represent the reduction in the hydrogen desorption zone. Electrolyte composition is 0.1 M NaOH, sweep rate was 10 $mV.s^{-1}$.

The partially covered Pt_{poly} was then removed from the electrolyte solution at fixed potential and transferred to another electrochemical cell, for the GEOR experiments.

After the experiments, in order to remove the adsorbed adatoms and recover a clean Pt surface, the Pt_{poly} was cleaned by immersion in aqua regia for 30 seconds, rinsed with ultrapure water and flame annealed, followed by quenching in ultrapure water.

The UPD of Cu on both electrodes was performed in a 0.5 M H_2SO_4 electrolyte, as well as the Bi UPD on Au_{poly}, while the Pb UPD on Au_{poly} was performed in 0.1 M NaOH. The metal salts used ($CuSO_4$, Bi_2O_3 or $Pb(NO_3)_2$) were at a fixed concentration of 10^{-3} M. The electrodes were immersed into the electrolyte at fixed potential, between 0.8 and 0.9 V, followed by negative scan until a high negative current was observed with minimal changes in the applied potential, indicating that multiple layers of the metal adatom were being deposited on the electrode (bulk

deposition). The lower potential limit was then set to a value immediately before the beginning of the bulk deposition to obtain a complete monolayer (θ = 1) of the metal adatom on the electrode surface. The electrode was polarized for 10 s at this potential, removed from the cell, rinsed with ultrapure water and transferred to a second cell for the GEOR measurements. In the second cell, the electrode was immersed into the electrolyte while polarized at 0.1 V, followed by positive scan until 1 V. A bismuth electrode was made by depositing bulk amounts of Bi atoms on an Au_{poly} electrode. The Au_{poly} electrode was used as the working electrode, and a Pt wire as a counter/reference electrode in a two-electrode arrangement, and a potential difference of – 2 V was applied for 20 min. This bulk Bi electrode had the same blank voltammogram as shown for Bi nanoparticles[63] in the literature. The Au electrode was chosen instead of Pt due to its higher double layer region, no interference from hydrogen adsorption and to its high onset potential for the GEOR (0.6 V for Au, while Pt has an onset potential of 0.4 V in alkaline media[21]).

3.3. High Performance Liquid Chromatography and on-line sample collection

The system for electrochemical measurements with on-line sample collection is shown in figure 10.

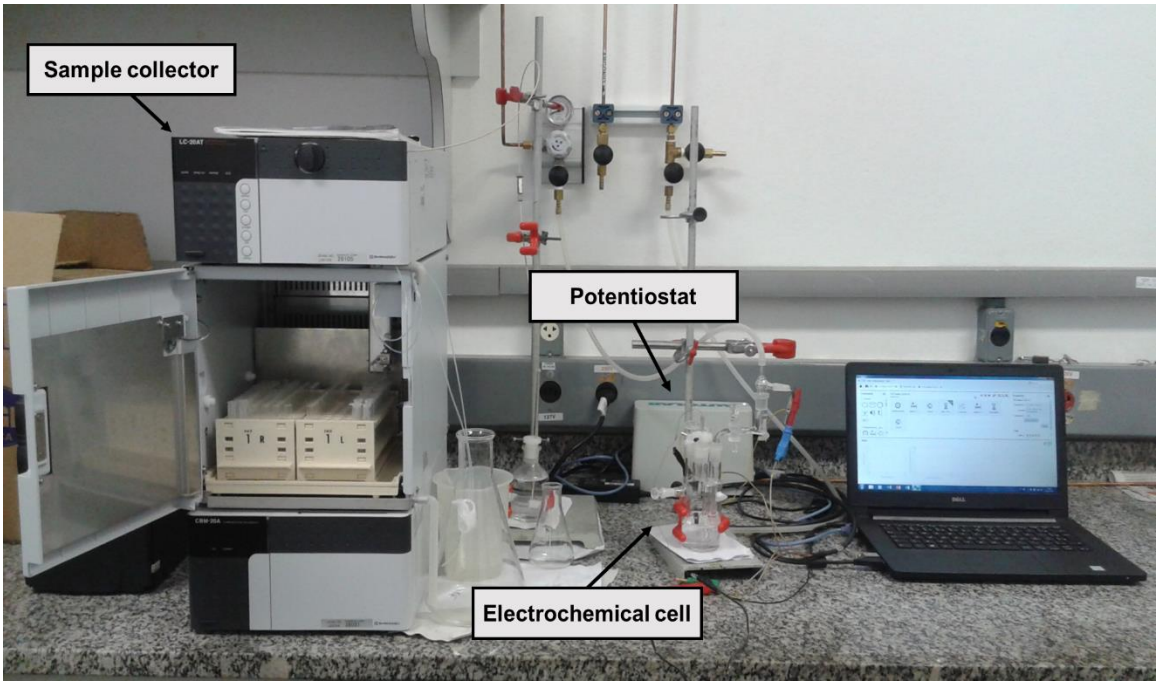

Figure 10: Experimental scheme of the electrochemical measurements couple with on-line sample collection.

The working electrode used during sample collection was a platinum (Pt_{disk}) disk (Alfa Aesar) with 0.9 cm diameter, cleaned in the same fashion as the Pt_{poly} electrode. The GEOR was performed using the hanging meniscus configuration on the working electrode. Samples were collected using a Shimadzu sample collector FRC – 10A by placing a PEEK capillary tip as close as possible to the working electrode (figure 11). The capillary was thoroughly rinsed with ultrapure water before insertion into the electrochemical cell. To avoid forming a lateral meniscus between the Pt_{disk} and the glass tube in which the PEEK capillary is contained, the Cu wire holding the Pt_{disk} was slightly bent, and the capillary tip was bent towards the center of the Pt_{disk}.

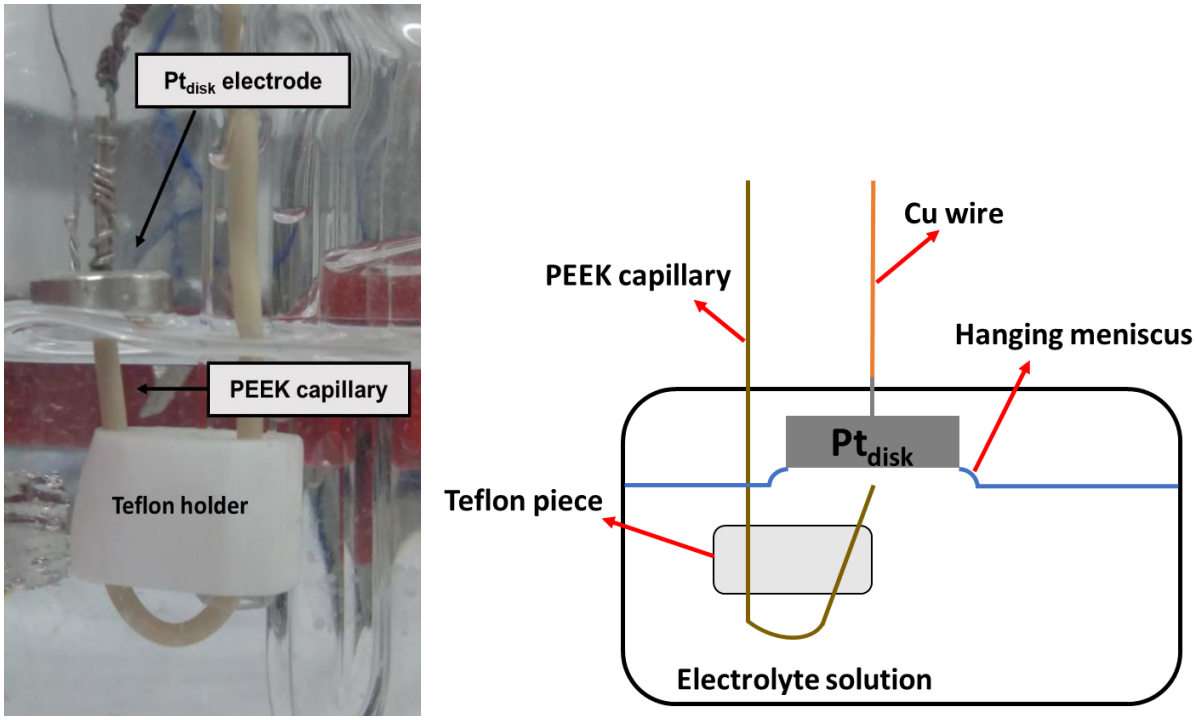

Figure 11: (left) PEEK capillary, connected to the sample collector, placed close to the Pt_{disk} surface, while being held at place by a Teflon piece; (right) scheme of the PEEK capillary placement.

The contact between the working electrode and electrolyte solution was made after polarization at 0.2 V. This potential was held for 3 min, followed by positive sweep to 0.85 V. The electrolyte composition was 0.1 M NaOH + 0.1 M GOH, and the sweep rate was 1 $mV.s^{-1}$. Samples were collected at a flow rate of 60 $\mu L.min^{-1}$, therefore each fraction collected corresponded to a 60 mV interval, when compared to the voltammogram. The collection was performed after 9 cycles at 10 $mV.s^{-1}$, to precondition the working electrode. Samples were stored in 0.5 mL eppendorf tubes and had their pH correct to 2, by addition of 20 µL of a H_2SO_4 solution, to prevent further oxidation of intermediates[42].

The HPLC experiments were performed in an Agilent series 1200 chromatograph, with a quaternary pump, a thermostatted column compartment, ALS autosampler, vacuum degasser and a refractory index detector, kept at 35°C. Three separation columns were used, in the following order: an Aminex HPX87-H and two Shodex Sugar SH1011. The columns were kept at 85°C, and a Bio-Rad 1250131

precolumn was used. Mobile phase was 0.5 mM H_2SO_4, with 0.6 mL.min^{-1} flow rate, and the injection volume was 20 µL.

3.4. In-situ Fourier Transform Infrared Spectroscopy experiments

In situ infrared experiments were performed in a glass cell using a reversible hydrogen electrode as the reference electrode and a gold wire as the counter electrode. The solutions were deaerated with Ar (N50, Air Liquide) and blanketed with this gas during the experiments. A Nexus 8700 (Thermo Scientific) spectrometer equipped with a MCT-A detector and a wire grid ZnSe polarizer (Pike Tech) was the instrument used. The cell was equipped with a CaF_2 (IRRAS) window beveled at 60º and placed at the top of a Veemax (Pike Tech.) reflectance accessory. All the potential-dependent spectra were collected with a resolution of 8 cm^{-1} and are presented in absorbance units (a.u.) as $-\log(R/Ro)$, where R and Ro represent, respectively, the reflectivity at the sample and reference potentials. Thus, positive and negative bands correspond, respectively, to gain or loss of species at the sample potential with respect to the reference potential. Dynamic experiments (rapid scan-RS) were carried out and the spectra were collected in a rapid scan mode while the electrode potential was swept at 2 mV·s^{-1}. The spectra recording took place after the electrode was preconditioned by 9 cycles at 10 mV.s^{-1}. In these experiments, each spectrum was the average of a set of 260 interferograms which were collected in a 50 mV interval. All the spectra are referred to the reference single beam spectrum collected in the glycerol-containing solutions at 0.10 V.

3.5. Chemicals

All chemicals were employed without previous treatment. The chemicals used in the electrochemical measurements, with and without on-line sample collection, were sulfuric acid (ISO, Emsure®), nitric acid (PA ACS, LS Chemicals), hydrogen peroxide (30% wt, LS Chemicals), hydrochloric acid (PA, Ls Chemicals), glycerol (ACS grade, Sigma-Aldrich), copper (II) sulfate pentahydrate (ACS, Merck), bismuth (III)

oxide (ReagentPlus®, Sigma-Aldrich), lead (II) nitrate (99.999% trace metal basis, Sigma-Aldrich), sodium hydroxide (semiconductor grade, 99.99% trace metal basis, Sigma-Aldrich) and potassium permanganate (PA ACS grade, Vetec Química). All solutions were prepared using ultrapure water (18.2 MΩ · cm @ 25ºC, Millipore).

The in-situ Fourier transform spectroscopy experiments were performed using the following chemicals: glycerol (99.9% CalbioChem), sodium hydroxide monohydrate 99.99% (Merck Suprapur®), bismuth (III) oxide 99.999% (Sigma-Aldrich), deuterium oxide 99.9% (Sigma-Aldrich) and ultrapure water (18.2 MΩ · cm, TOC 50 ppb max, Elga Vivendi).

The standard chromatograms for identification of several oxidation products (fig. S1), calibration curves (fig. S2) and standard FTIR spectra (fig. S3) were obtained using the following chemicals: sulfuric acid (ISO, Emsure®), sodium hydroxide (semiconductor grade, 99.99% trace metal basis, Sigma-Aldrich), glycerol (ACS grade, Sigma-Aldrich), 1,3-Dihydroxyacetone dimer (97%, Sigma-Aldrich), D-glyceric acid calcium salt dihydrate (99%, Sigma-Aldrich), DL-Glyceraldehyde (≥ 90%, Sigma-Aldrich), Glycolic acid (99% ReagentPlus®, Sigma-Aldrich), sodium mesoxalate monohydrate (≥ 98.0%, Sigma-Aldrich), glyoxylic acid monohydrate (98%, Sigma-Aldrich), tartronic acid (97%, Sigma-Aldrich), oxalic acid (99%, anhydrous, Sigma-Aldrich) and sodium carbonate (99.5%, Labsynth).

4. Results and Discussion

4.1. Surface Modification via Underpotential Deposition

The voltammetric profiles for the UPD of Bi, Pb and Cu on Au_{poly} and of Cu on Pt_{poly} are shown in Figure 12. Bi and Pb adsorb irreversibly on Pt, and their only effect on the voltammogram of Pt_{poly} is the reduction of the hydrogen adsorption-desorption zone, in addition to a reversible peak associated to their redox process on the electrode surface[56,57].

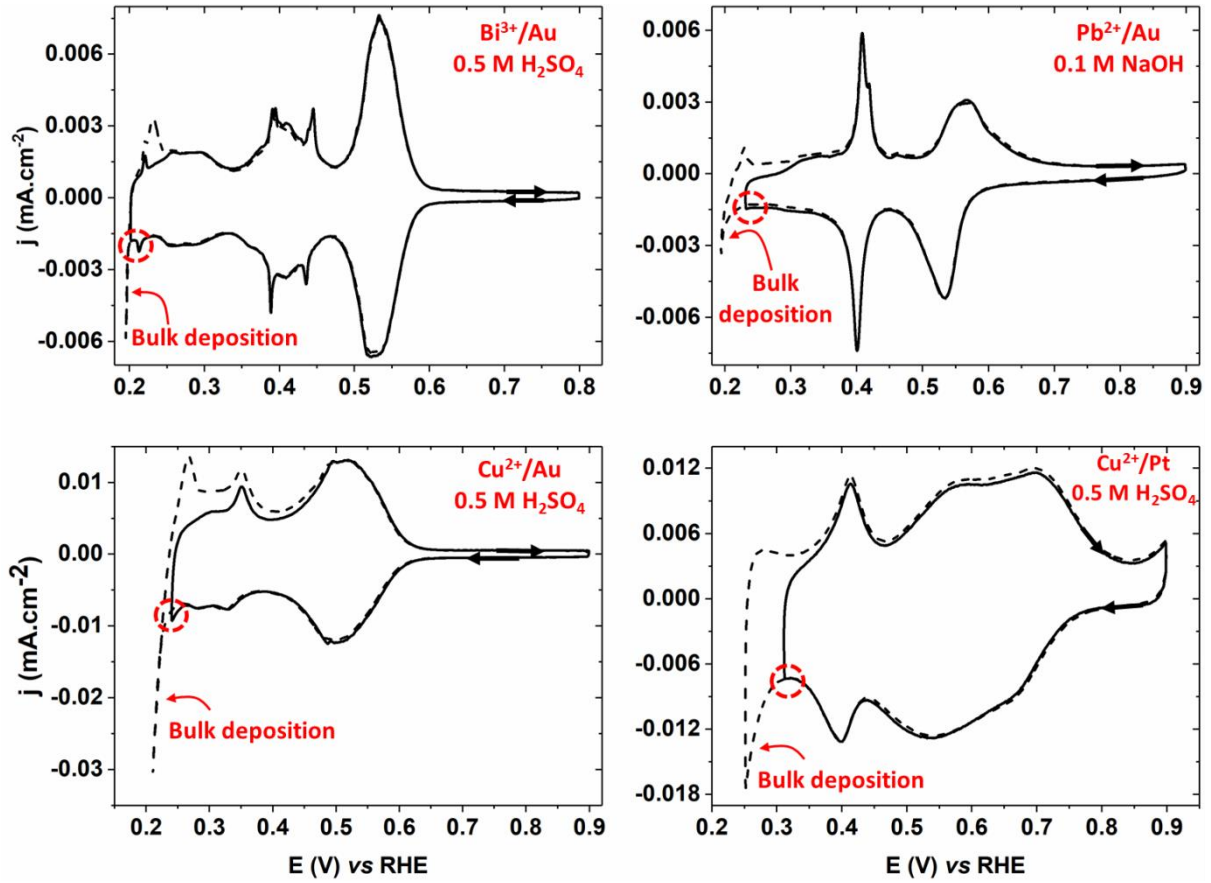

Figure 12: Voltammetric response for the UPD of Bi on Au_{poly} (top left), Pb on Au_{poly} (top right), Cu on Au_{poly} (bottom left) and Cu on Pt_{poly} (bottom right), exhibiting both the limit for monolayer formation (full line) and the bulk deposition (dashed line). The base electrolyte is 0.5 M H_2SO_4 for Bi and Cu deposition, and 0.1 M NaOH for Pb deposition, in addition to 10^{-3} M of the corresponding metal salt (Bi_2O_3, $Pb(NO_3)_2$ or $CuSO_4$). Sweep rate is 10 $mV.s^{-1}$ for all measurements. The arrows show the scan direction, and the red dotted circle indicates the potential for monolayer coverage.

The UPD process is seen as a negative current during the negative scan, on what was originally the electric double layer region of both electrodes, as well as the hydrogen adsorption/desorption zone of Pt. This negative current is attributed to the reduction and deposition of the metallic ions (Cu^{2+}, Bi^{3+} or Pb^{2+}). Each adatom-substrate pair follows distinct deposition mechanism, being both the thermodynamic and kinetics of the process influenced by the electrolyte composition, temperature, etc.

When the applied potential reaches that of monolayer formation (red dotted circles in figure 12), the current remains approximately constant. Further reduction of

the applied potential generates a high reduction current (dashed lines in figure 12) associated with the bulk (massive) deposition of the adatom species, i.e., a 3D growth of the metal phase is taking place at the electrode surface[33]. Since our objective is to deposit complete or partial monolayers of the metal adatoms, this study was done in order to determine the potential window in which the electrodes could be modified.

4.2. Irreversible adsorption of bismuth on platinum

Due to the fact that in this work we studied the GEOR in presence of different concentrations of Bi ions in solution, we studied the changes in the surface of Pt_{poly} as it is cycled in a solution containing Bi ions. Figure 13 shows the effect of cycling the Pt_{poly} electrode in alkaline media with varying concentrations of Bi^{3+} in solution, as indicated on the inset of each voltammogram. The electrode was polarized at 0.3 V before immersion into the electrolyte and held at this potential for 3 min, followed by negative scan to 0.2 and positive scan to 0.85 V.

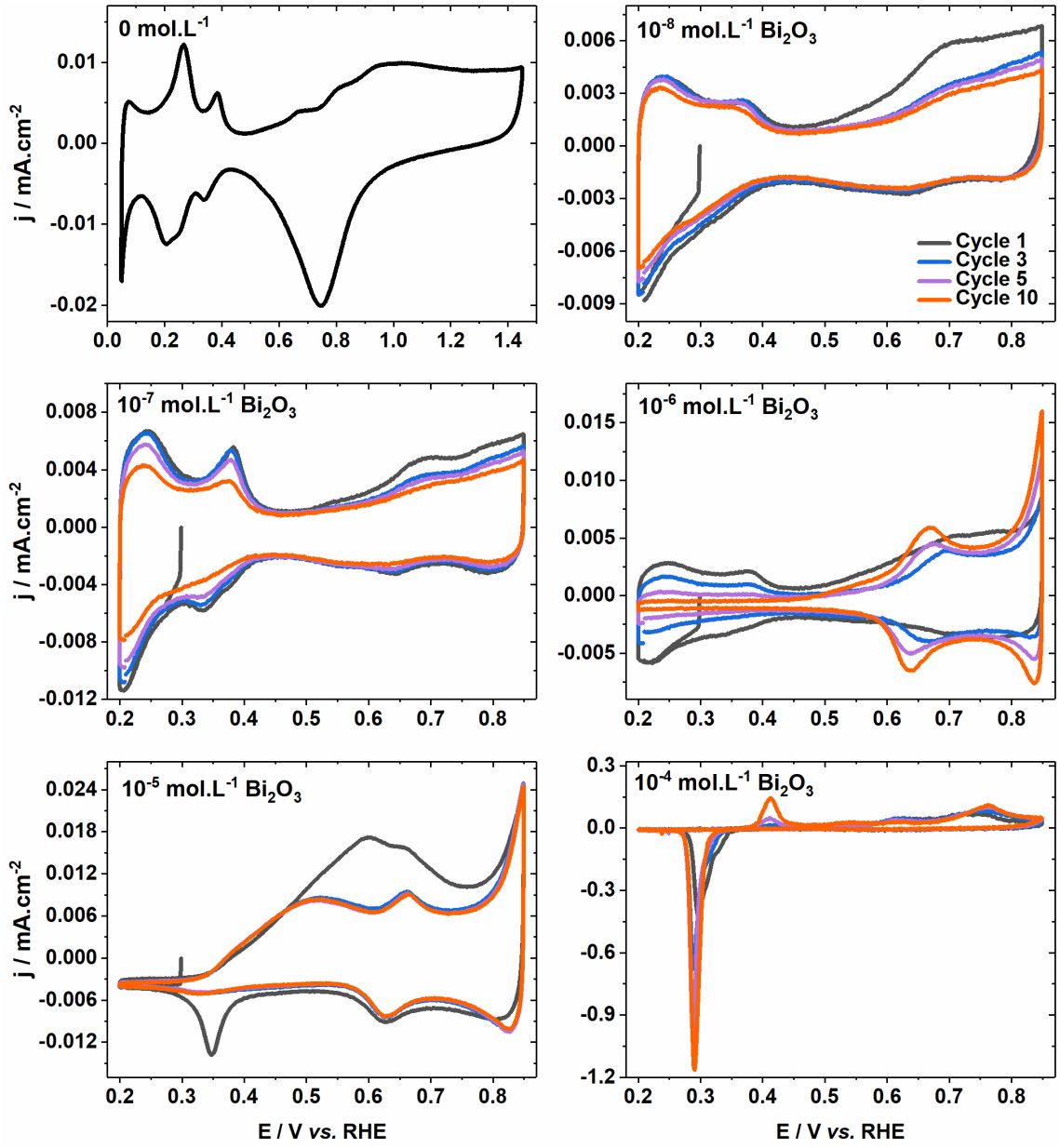

Figure 13: Effect of cycling the Pt_{poly} electrode in 0.1 M NaOH with varying concentrations of Bi_2O_3, as shown on the inset of each voltammogram. Sweep rate was 10 $mV.s^{-1}$ during all measurements.

The results shown in figure 13 reveal that the Pt_{poly} electrode was not completely covered by Bi when 10^{-8} or 10^{-7} M Bi_2O_3 was added to the electrolyte, because the hydrogen adsorption/desorption region can still be observed after 10 cycles. The calculated value of bismuth coverage (θ_{Bi}) was 0.79 and 0.73 for the 10^{-8} and 10^{-7} M Bi_2O_3, respectively. With 10^{-6} M Bi_2O_3 in solution, however, a complete electrode coverage (θ_{Bi} = 1) is achieved around the 5th cycle, evidenced by the

complete blockage of the hydrogen region and the new reversible peaks at 0.63 V, attributed to the Bi oxidation to $Bi(OH)_2$ and its subsequent reduction to Bi on (111) sites[56,64]. A completely different behavior is observed for 10^{-5} M Bi_2O_3. The electrode is completely covered with Bi from the beginning of the experiment, and a broad oxidation region in the 0.5 – 0.8 V range is observed for the 1st cycle, as well as a reduction peak centered at 0.35 V. These features disappeared by the 3rd cycle, and the voltammetric profile stabilized. Lastly, at 10^{-4} M, the voltammogram did not stabilize even after 10 cycles, as seen by the continuous increase in a stepped cathodic peak at 0.30 V, attributed to a constant increasing of the reduction of massive Bi oxide/hydroxide and the consequent continuous deposition of Bi. Indeed, this profile is similar to the blank voltammogram obtained for a Bi electrode in 0.1 M NaOH (figure 14), the anodic peak centered around 0.65 V, observed with 10^{-6} and 10^{-5} M Bi_2O_3 in figure 13, are in agreement with the Bi oxidation region observed in figure 14.

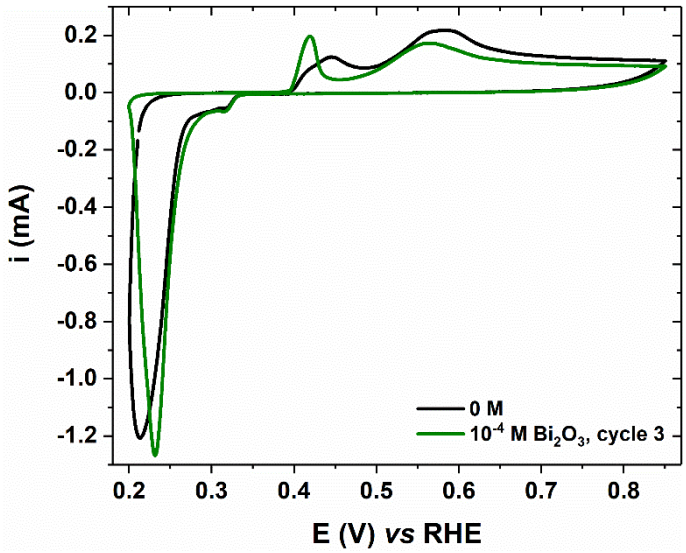

Figure 14: Voltammetric response obtained for a bulk Bi electrode in 0.1 M NaOH, in the absence (black) and presence of 10^{-4} M Bi_2O_3 (green). Scan rate is 10 $mV.s^{-1}$.

4.3. Glycerol electrooxidation on gold surfaces modified by metal adatoms

The GEOR on the Au_{poly} modified with a full monolayer of underpotentially deposited Cu, Bi and Pb is shown in figure 15. The electrode was polarized at 0.1 V and immersed into the electrolyte at this potential, and after 3 min a positive scan until 1 V was performed.

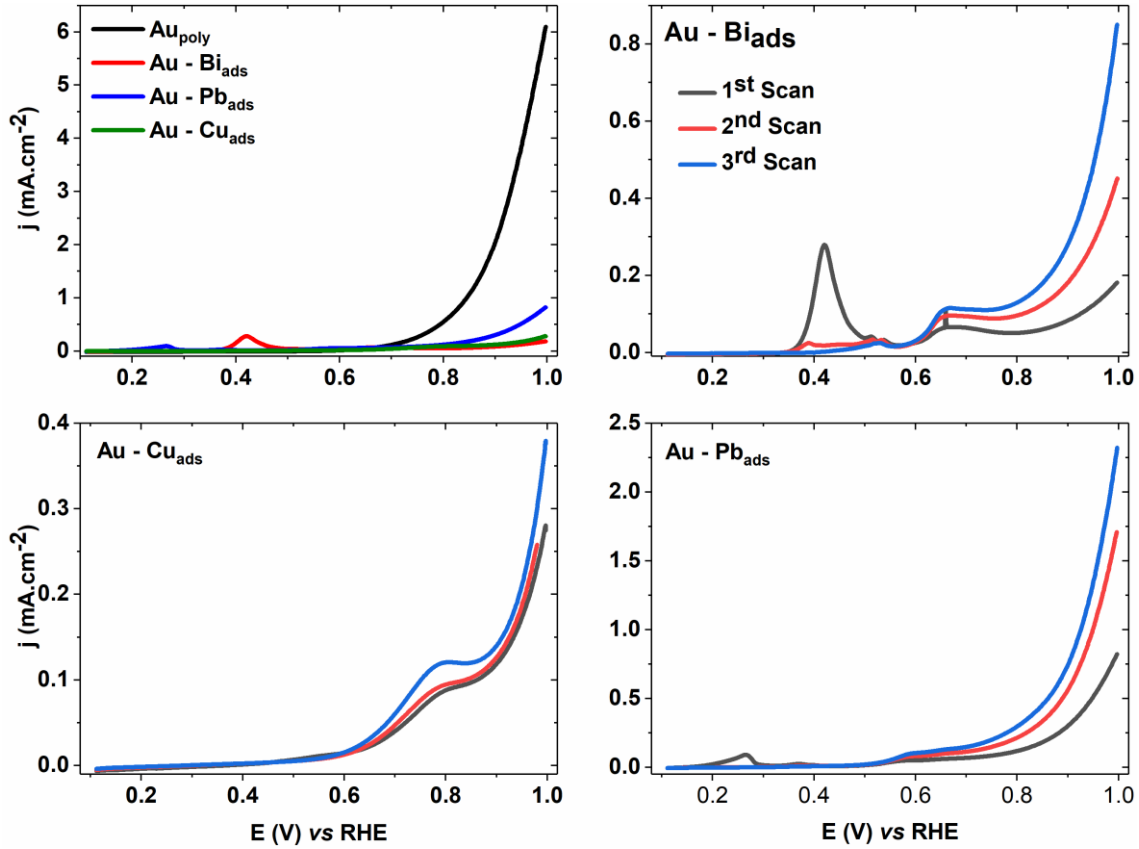

Figure 15: (Top left) Positive scan of the 1st cycle of the voltammogram recorded for the GEOR on the Au_{poly} electrode modified by a full monolayer of Bi (red), Cu (green) and Pb (blue). First three positive-going scans of the GEOR in Au_{poly} modified by Bi (top right), Cu (bottom left) and Pb (bottom right). In all measurements, the electrolyte composition was 0.1 M NaOH + 0.1 M GOH, and the sweep rate was 10 $mV.s^{-1}$.

Initial examination of figure 15 indicates that the Au_{poly} electrode is completely deactivated for the GEOR after a full monolayer of the metal adatoms is deposited on its surface. The peaks near 0.2 and 0.4 V for the Au-Pb and Au-Bi systems, respectively, were attributed to the oxidation of those metals on the electrode

surface. Cycling the electrode in the potential window used in figure 15 revealed a continuous increase in the current density for the three electrodes. After several cycles, the electrodes recover the activity of Au_{poly}, indicating that the adatoms leave the electrode surface. Repeating these measurements with partial electrode coverage yielded similar results, i.e., the Au electrode was also deactivated and the diminution of the activity was proportional to the coverage.

Out of the metals chosen to modify the electrode surface, Cu is expected to remain adsorbed on the surface of Au even at high potentials, in its oxidized Cu(II) form, forming a monolayer of CuO on the electrode surface[65], which would explain why the recovery of the Au_{poly} is the slowest at this system, as seen on the slow increase of the current density in figure 15. The Pb atoms, on the other hand, seem to leave the Au electrode easily, evidenced by the fact that the current densities for the 3rd cycle are over two times higher than observed in the 1st cycle, although part of the Pb adatoms is known to irreversibly adsorb on Au[66]. Bi on Au shows a similar behavior as Pb [67,68].

As previously mentioned, Au(OH) formation is considered necessary to the GEOR on Au electrodes[39,41]. We hypothesize that the reduction in the activity of the electrodes is due to the fact that when the adatoms were deposited on the electrode surface, they occupied the available active sites (one, two and three sites for Cu, Pb and Bi, respectively[67]), diminishing the availability of Au(OH) and reducing the electrode activity. These results confirm that the GEOR on Au occurs in a completely different way than on Pt, as we will see in the next section.

4.4. Glycerol electrooxidation on platinum surfaces

4.4.1. Copper-modified platinum

The results for the GEOR on Pt_{poly} modified by UPD of Cu adatoms is shown in figure 16 below. The measurements were performed in the same way as previously described for the GEOR on Au_{poly} modified by adatoms.

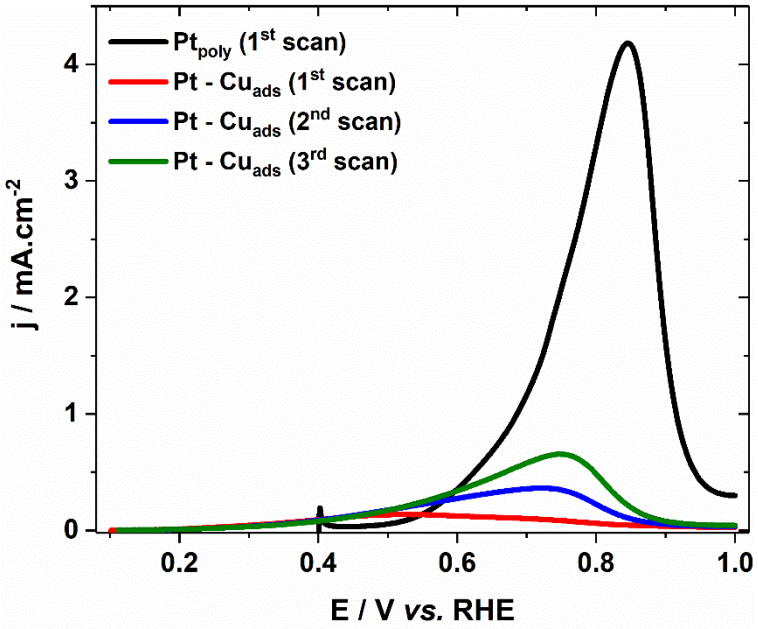

Figure 16: Positive scans of the of the 1st cycle of the voltammogram recorded for the GEOR on Pt_{poly} (black) and the first three scans of the Cu-modified electrode (red, blue and green). Electrolyte composition is 0.1 M NaOH + 0.1 M GOH, and the scan rate used was 10 mV.s^{-1}.

Similar to the Au-Cu system, Cu also deactivates the Pt_{poly} electrode for the GEOR in alkaline media, both at full and partial electrode coverage. Continuous cycling did not increase the current densities, indicating that the adsorbed Cu atoms did not leave the electrode surface in the specified potential window.

The fact that even low quantities of Cu negatively affect the electrode activity is a clear evidence that there must be an electronic effect over Pt atoms that modified the binding energy of the intermediates of the reaction in a non-favorable way. DFT studies and X-rays absorption techniques could help to clarify this point.

4.4.2. Bismuth-modified platinum

The impact of partial Bi coverage on the Pt_{poly} electrode for the GEOR in alkaline media is shown in figure 17. As was stated before, Bi was irreversibly adsorbed by immersion of the Pt_{poly} electrode in an acidic solution at open circuit, rinsed with

ultrapure water and a blank voltammogram was recorded in order to determine θ_{Bi}. Afterwards, the electrode was transferred to a second cell where the GEOR was performed.

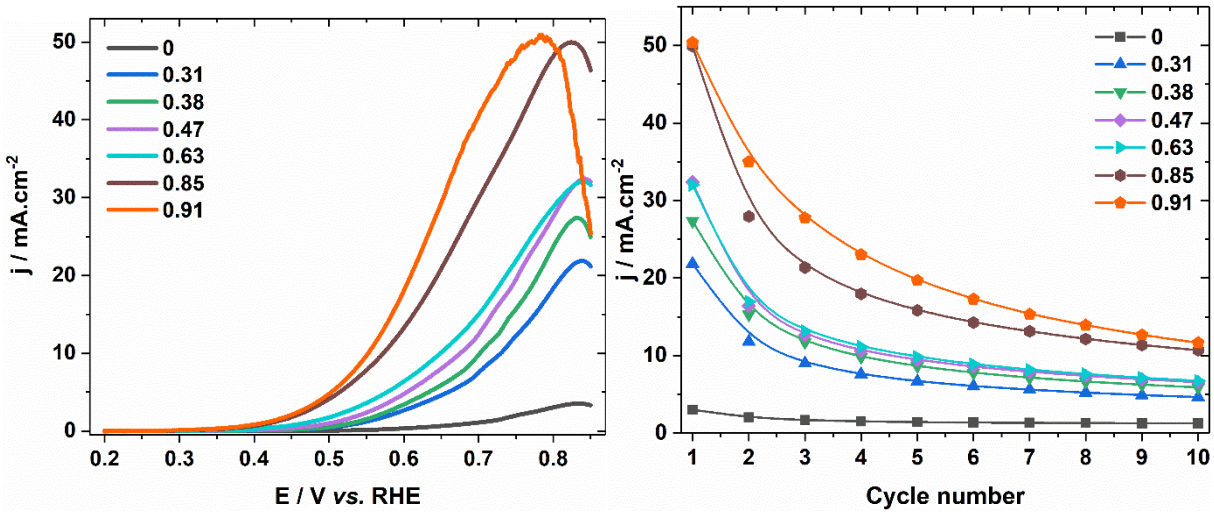

Figure 17: (left) Positive-going scan of the 1st cycle of the voltammetric profile obtained for the GEOR in alkaline media on the Bi-modified Pt_{poly} electrode, at different values of θ_{Bi}; (right) j_{peak} evolution with cycle number, for the same values of θ_{Bi} shown in the left image. Electrolyte composition was 0.1 M NaOH + 0.1 M GOH, and the scan rate was 10 $mV.s^{-1}$.

The results indicate that Bi impact is noticeable even at low coverage values ($\theta_{Bi} < 0.50$). Although j_{peak} had a considerable increase during the initial cycles for all values of θ_{Bi} examined, it continuously diminishes with electrode cycling, tending to the behavior of Pt_{poly}. Besides the impact in j_{peak}, the onset of the reaction also shifted to lower potentials when θ_{Bi} increased, by around 200 mV when $\theta_{Bi} = 0.90$, indicating again the promoting effect of the deposition of Bi for the GEOR.

The unmodified Pt_{poly} electrode also showed deactivation with continuous cycling, which has been attributed to the adsorption of CO[69], both linearly and bridge-bonded, and to the adsorption of GOH residues[39], likely to be acyl intermediates, as shown in recent literature reports in alkaline media[51]. Thus, even if the results showed in figure 17 suggest that θ_{Bi} decreases along cycling, it cannot be discarded the poisoning of the modified surfaces.

The impact of θ_{Bi} on the Pt activity was also evaluated by examining changes in the current density with electrode coverage, as seen in figure 18.

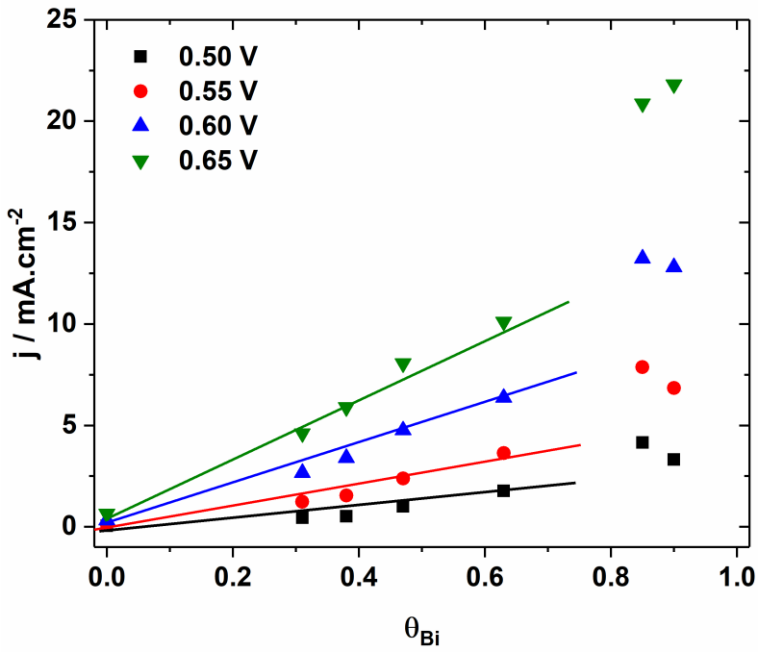

Figure 18: Relationship between current density and electrode coverage at different electrode potentials. Data extracted from the left image in figure 17.

The data in figure 18 shows that current density has a near linear relationship with electrode coverage in the range $0 < \theta_{Bi} < 0.60$, for all potentials analyzed. This linearity could be an indicator that Bi enhances the Pt activity by means of a third body effect[55]. This effect consists of a selective blockage of catalyst active sites by adatom deposition, which is advantageous when the unmodified sites would otherwise participate in parallel reactions leading to formation of poisoning products or intermediates. In the case of Pt, CO is a well-known poisoning intermediate, formed during the oxidation of several organic molecules[70]. The third body effect is observed during methanol oxidation on the Pt-Bi system in acidic media[30], where poison formation (CO adsorption) decreases linearly with θ_{Bi}, coming to a stop at $\theta_{Bi} > 0.23$.

As was stated before, the electrode deactivation can be caused by poisoning intermediates, and also by the progressive loss of the adatom layer[56,58,71].

Therefore, the GEOR was investigated in the presence of Bi^{3+} ions in the electrolyte, in order to have a constant supply of adatoms (figure 19).

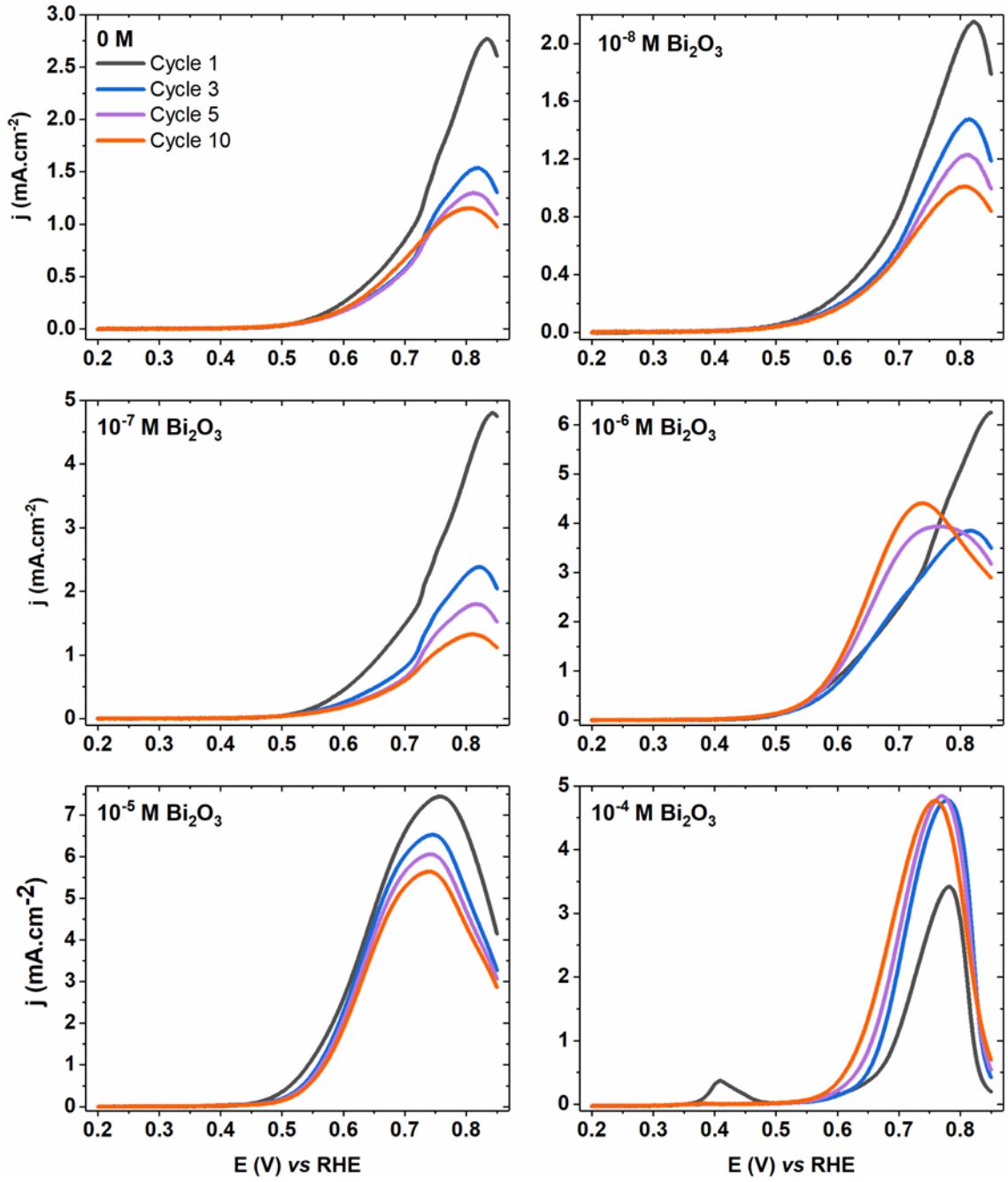

Figure 19: Selected positive-going scans for 10 cycles of the GEOR in alkaline media on a Pt_{poly} electrode, with varying concentrations of Bi^{3+} in the electrolyte. Base electrolyte composition is 0.1 M NaOH + 0.1 M GOH, and the scan rate was 10 $mV.s^{-1}$.

Results in figure 19 show an increase in catalytic activity with increasing bismuth concentration, until 10^{-5} M Bi_2O_3, after which there is both a decrease in j_{peak} and increase in E_{peak}.

At low Bi concentrations (10^{-8} and 10^{-7} M), the voltammetric profile obtained is similar to what was recorded in absence of Bi (0 M in figure 19), as well as to the partial electrode coverage experiments shown in figure 11. At the 10^{-6} M concentration, however, a change in the voltammetric response is observed during continuous cycling. The initial cycles resemble the GEOR response for low Bi concentrations (0 to 10^{-7} M), however the last cycles resemble the response shown for the systems with a higher Bi (10^{-5} and 10^{-4} M) concentration.

Figure 13 enables the rationalization of the results in figure 19. At low Bi concentrations (10^{-8} and 10^{-7} M) the electrode is only partially covered by Bi. Thus, the results resemble those obtained with partially covered electrodes. The complex behavior at at 10^{-6} M is due to the fact that in the first cycles the electrode is only partially covered by Bi, hence the response is similar to the one shown for the low Bi concentration systems and for partial θ_{Bi} values. During the final cycles, the Bi monolayer is complete, then, the response shown is similar to that of the higher Bi concentration systems.

To understand the electrocatalytic activity of bulk Bi, which could be present in the experiments performed with 10^{-4} M of Bi ions, the GEOR was performed at a Bi electrode (Figure 20), both in absence and presence of 10^{-4} M Bi_2O_3 in solution.

The results are similar to those obtained in absence of GOH, indicating that bulk Bi is inactive to the GEOR. Besides, the features observed in figure 20 are essentially equal to those shown in figure 14, confirming that in presence of 10^{-4} M Bi ions there is a continuous deposition of Bi atoms on Pt, which explains the reduced current density observed when the concentration of Bi ions is increased from 10^{-5} to 10^{-4} M.

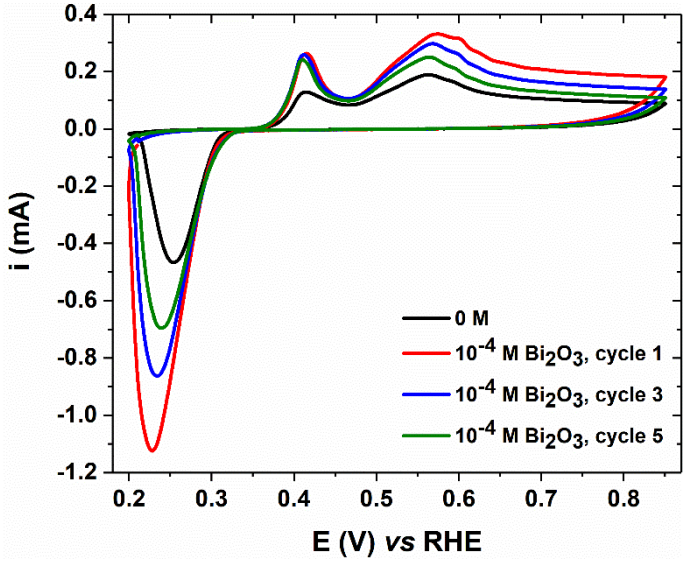

Figure 20: GEOR profile at a Bi electrode, in absence (black) and presence of Bi^{3+} ions (red, blue and green), where a few selected cycles are shown. Electrolyte composition was 0.1 M NaOH + 0.1 M GOH, with 10^{-4} M Bi_2O_3 in the red, blue and green curves. Sweep rate was 10 $mV.s^{-1}$.

The stability of the performance of these Pt-Bi systems was examined by evaluating the changes in E_{peak} and j_{peak} with cycle number. These plots are shown in figure 21.

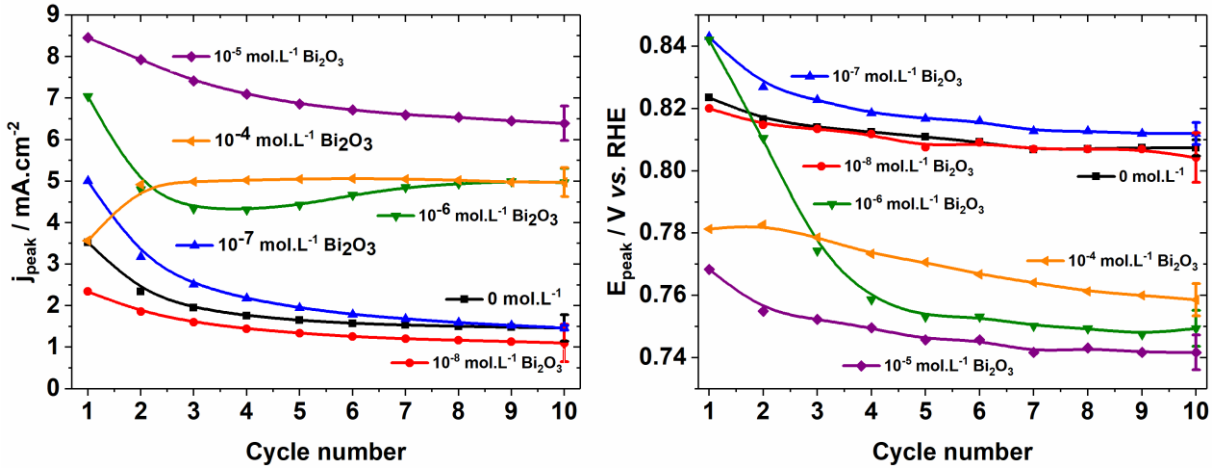

Figure 21: Plots of j_{peak} (left) and E_{peak} (right) vs. cycle number for the GEOR on a Pt electrode with different Bi^{3+} concentrations in solution: 0 M (black), 10^{-8} M (red), 10^{-7} M (blue), 10^{-6} M (green), 10^{-5} M (purple) and 10^{-4} M (orange). Data extracted from the voltammograms shown in figure 19.

The drop in j_{peak} with continuous cycling for the systems with Bi in solution in figure 19 is significantly smaller than in the experiments with partial electrode coverage, shown in figure 17. The system with 10^{-5} M Bi_2O_3 in the electrolyte showed both the highest j_{peak} (5-6 times bigger than for 0 M Bi_2O_3) and lowest E_{peak} values among all Bi concentrations examined, for all cycles. This system also showed more stability than the unmodified Pt_{poly} electrode, evidenced by a 25% drop in j_{peak} by the 10^{th} cycle, when compared to j_{peak} on the 1^{st} cycle, while for the GEOR in absence of Bi showed a 60% drop in j_{peak}. Those results lead to the conclusion that 10^{-5} M Bi_2O_3 was the optimum concentration of Bi in order to enhance the GEOR on a Pt_{poly} electrode in alkaline media.

4.4.2.1. In-situ Fourier Transform Infrared Spectroscopy Analysis

The *in-situ* FTIR measurements were done with a Pt_{poly} electrode, both in presence and absence of 10^{-5} M Bi_2O_3 in solution. The spectra recorded for the Pt and Pt-Bi electrodes using deuterated water (D_2O) is shown in figure 22.

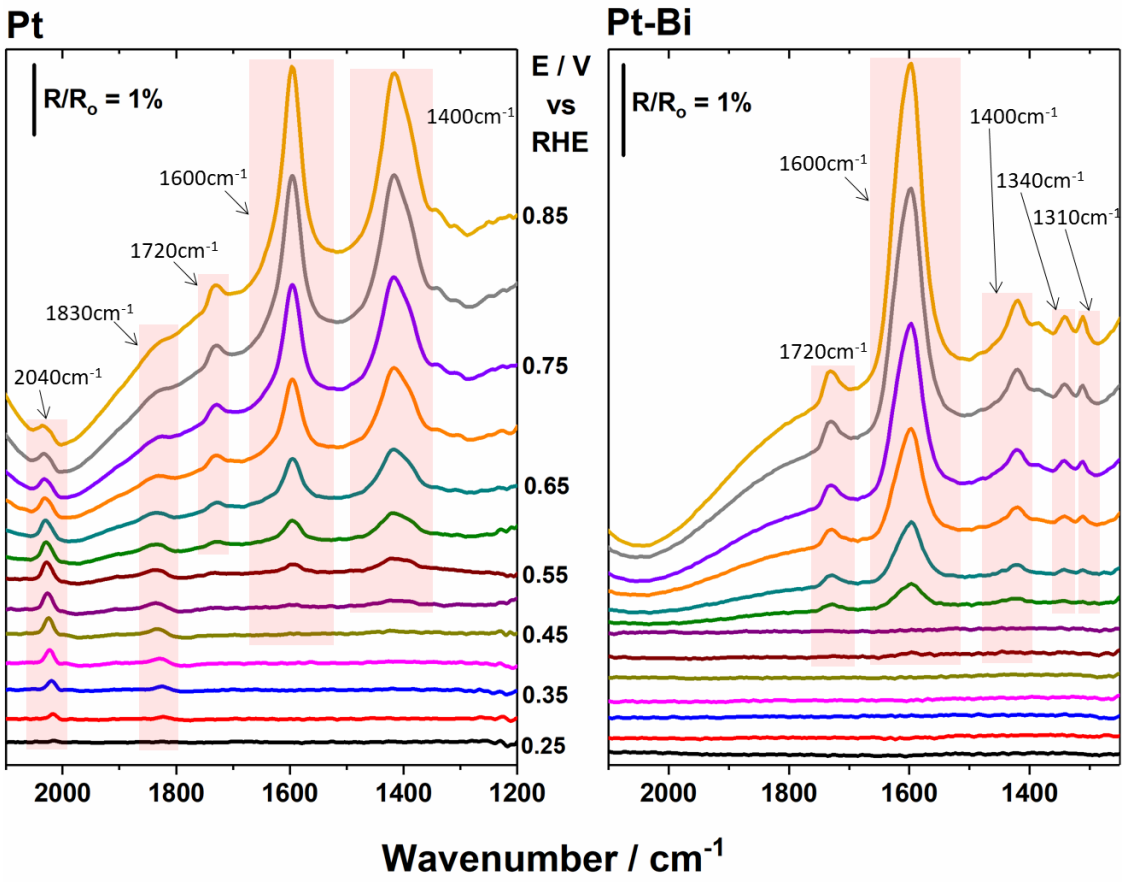

Figure 22: Potential-dependent FTIR spectra for the clean (left) and Bi-modified (right) Pt electrode. Electrolyte composition was 0.1 M NaOH + 0.1 M GOH, with 10^{-5} M Bi_2O_3 added for the Bi modification. Scan rate was 2 mV.s^{-1}.

The GEOR on Pt/C nanoparticles in similar conditions generated six main absorption bands in the 1100-1600 cm^{-1} range, according to literature reports[72]. We only observed two bands in this region, which we attribute mainly to the difference in catalyst of choice, where Pt/C nanoparticles have a significantly higher surface area than a polycrystalline Pt disk, allowing better peak resolution

The spectra recorded for the clean Pt electrode (figure 22, left) shows that CO is adsorbed on the electrode surface since the beginning of the experiment, as seen by the bands at 1830 and 2040 cm^{-1}, assigned to multiply and linear-bonded CO on Pt, respectively[73]. These bands are present since the beginning due to the electrode preconditioning, i.e. 9 cycles at 10 mV.s^{-1} prior to recording the spectra at 2 mV.s^{-1}. The band at 1720 cm^{-1} corresponds to the stretching of a carbonyl (C=O) group[48,49], and it is only observed after 0.60 V. From the spectra recorded for various oxidation

products (cf. fig. S1), oxalate, tartronate, glyoxylate and glycolate all produce a band at this wavelength. The lack of a feature at 1630 cm^{-1} rules out tartronate and oxalate, making glyoxylate and glycolate the most suitable candidates for the 1720 cm^{-1} band.

The band at 1600 cm^{-1} was assigned to the stretching of the COO^- group, indicating formation of glycerate ions[11,72,74], according to the following reaction:

$$CH_2OH - CHOH - CH_2OH + 5OH^- \rightarrow CH_2OH - CHOH - COO^- + 4H_2O + 4e^- \quad (12)$$

Substitution of H_2O for D_2O suppressed the H-O-H stretching mode of water at 1600 cm^{-1} [73,74], allowing a better resolution of this feature (the spectra recorded with H_2O is shown in fig. S2). In addition to glycerate, both formate and mesoxalate show a strong band at 1600 cm^{-1}. However, only small amounts of formate are generated on Pt in alkaline media in our potential window, while mesoxalate is only a proposed reaction product, as it has not been previously detected[21]. Thus, glycerate is the most suitable candidate for this feature. Other products with a band at 1600 cm^{-1} are di-hydroxyacetone, glyceraldehyde, glyoxylate and glycolate, however all of them have only a small feature in this region, significantly smaller than that of glycerate. In particular, glyceraldehyde and di-hydroxyacetone can only be properly identified below 1300 cm^{-1}, which is difficult to analyze due to superimposition of bands from several compounds.

The large band centered at 1400 cm^{-1} is first detected around 0.50 V, and indicates the presence of carbonate (CO_3^{2-}) ions[74], originating from GOH complete oxidation:

$$CH_2OH - CHOH - CH_2OH + 20OH^- \rightarrow 3CO_3^{2-} + 14H_2O + 14e^- \quad (1)$$

In the GOH complete oxidation, seen in reaction (1), three CO_2 molecules are formed, however in alkaline media they combine with the hydroxyl ions into carbonate ions, and are detected as such during *in-situ* FTIR measurements[21].

Comparing the spectra registered for the Pt-Bi electrode (fig. 22 right) with that of clean Pt (fig. 22 left), several different features are observed. In the presence of Bi, no bands associated with CO adsorption are observed, confirming the hypothesis that Bi enhanced the activity of Pt by means of a third-body effect, blocking the CO adsorption on the Pt surface, as was thought from the data in figure 17[13]. The band at 1720 cm^{-1} is now more prominent than in the unmodified Pt electrode, and is first

detected at the same potential. The COO^- stretching band at 1600 cm^{-1} is now more intense, while the CO_3^{2-} band at 1400 cm^{-1} is now significantly smaller. Two bands at 1340 and 1310 cm^{-1} are detected at 0.60 V, previously seen as shoulders of the carbonate band in the clean Pt electrode. Identification of these bands was note possible due to the superimposition of several compounds in this region (cf. fig. S1).

From the COO^- stretching at 1600 cm^{-1}, glycerate ions[11] were identified as the main oxidation products for the GEOR on the Pt-Bi catalyst. To confirm this hypothesis, HPLC measurements were performed in order to identify and quantify the oxidation products of the GEOR on the Pt-Bi catalyst.

4.4.2.2. High-Performance Liquid Chromatography Analysis

The HPLC measurements were performed using the Pt_{disk} electrode, using a clean and Bi-modified electrode. The chromatographs for those systems are shown in figure 23.

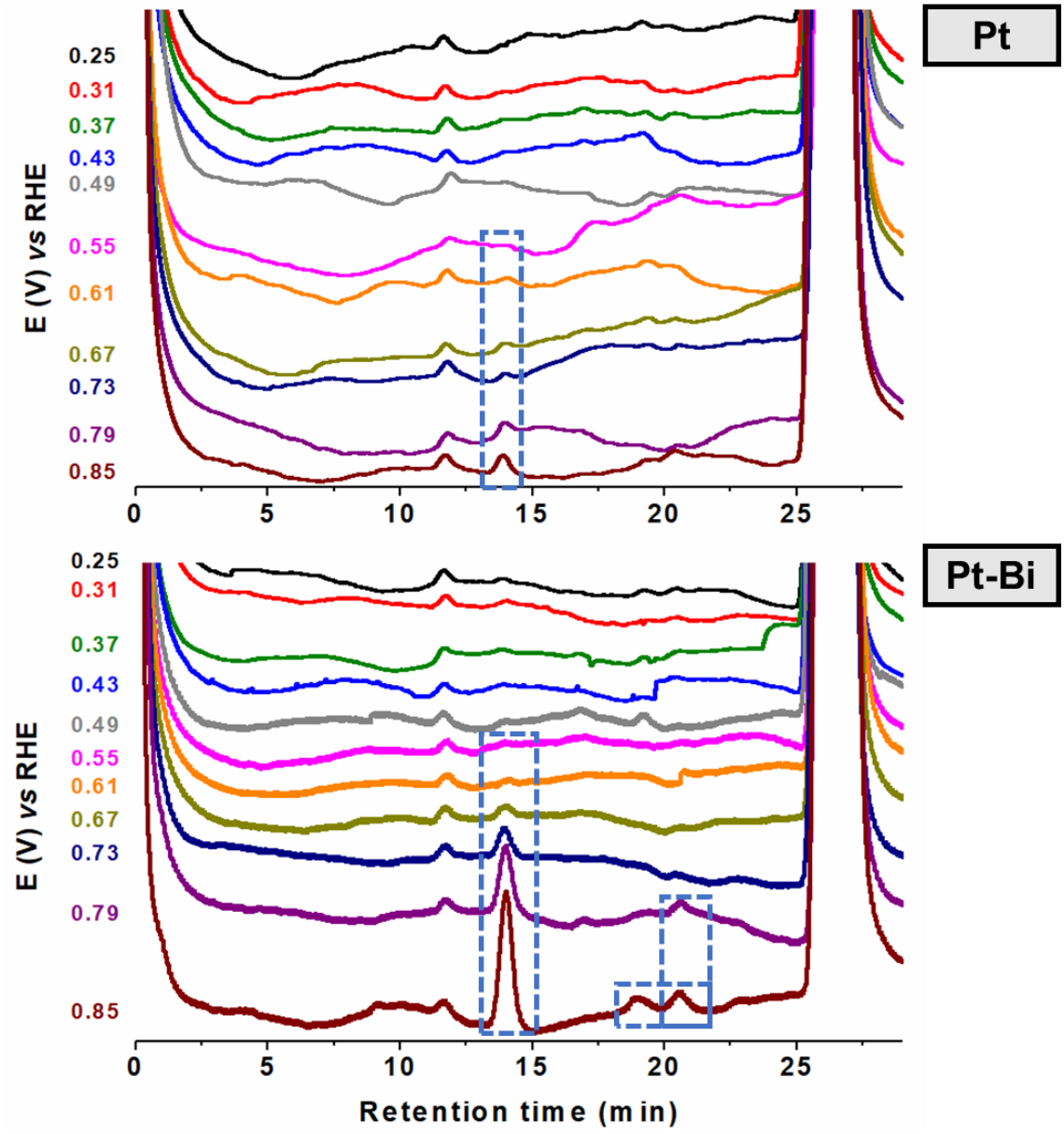

Figure 23: Chromatographs obtained after HPLC analysis of the samples collected during the electrochemical sweep in absence (top) and presence (bottom) of Bi in the electrolyte, highlighting the peaks where products were identified. Retention times calculated with respect to the mobile phase (H_2SO_4).

The peak at 11.6 min was labeled as a characteristic peak of the electrolyte, since it was present since the beginning of the experiment, in a potential range where Pt does not oxidize GOH[21]. The peak at 14 min was identified as being the glycerate ion (fig. S3), detected on both chromatograms from 0.55 V upwards. In the Bi-modified electrode, this peak is significantly more intense. These observations agree with the

previous assignment of the 1600 cm^{-1} band from the FTIR spectra (fig. 22) to the glycerate ion. The peaks at 18.9 and 20.5 min were observed only after the Bi modification, and they were identified as glycolate and formate ions (cf. fig. S3). This indicates that the 1720 cm^{-1} band (fig. 22) is due to glycolate, as glyoxylate was not detected. Even though this feature was observed on the clean Pt electrode, we are unable to ascertain it because we were unable to detect glycolate from the HPLC measurements, likely because its concentration was below our resolution limit (50 µM).

These observations are in agreement with the results published by Kwon and co-workers[21], where they identified glyceric acid production starting at 0.6 V *vs* RHE for a Pt electrode in alkaline media, and having its maximum concentration at 0.85 V, the E_{peak} of the GEOR on Pt. Only small amounts of glycolic and formic acid were detected, since their production starts at high potentials, while the Pt surface starts to oxidize.

4.4.2.3. Electrochemical, chromatographic and spectroscopic results

Figure 24 shows the positive potential scan for Pt and Pt-Bi (A and B) together with the integration of the FTIR bands (C and D) and the HPLC bands (E and F) at different electrochemical potentials.

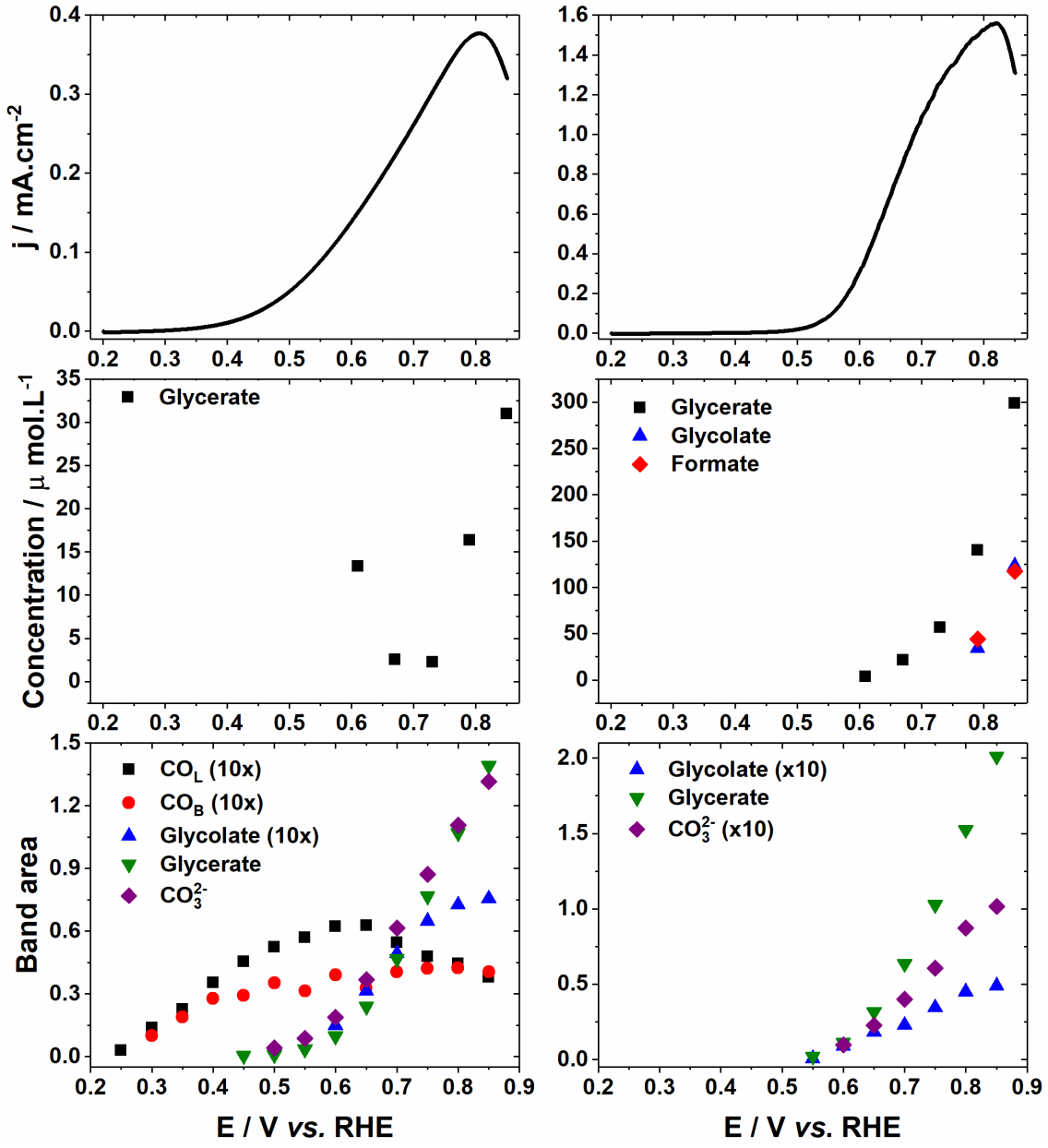

Figure 24: Results obtained for the GEOR on the Pt (left) and Pt-Bi (right) catalysts; (top row) positive sweep of the GEOR during on-line sample collection using a clean (left) and Bi-modified (right) Pt electrode. The electrolyte composition was 0.1 M NaOH + 0.1 M GOH, with 10^{-5} M Bi_2O_3 for the Bi modification, with a sweep rate of 1 $mV.s^{-1}$; (middle row) Concentration evolution of the oxidation products with applied potential, using data extracted from fig. 22; (bottom row) Band areas of CO_3^{2-}, C=O, linearly (CO_L) and bridge-bonded (CO_B) CO on Pt, as a function of electrode potential, using data from figure 22.

Results in fig. 24 indicate that the measured current during the electrochemical experiments for the GEOR on a clean Pt electrode is mostly due to glycerate and carbonate ions, corresponding to the oxidation a primary hydroxyl group and the GOH complete oxidation, respectively. As previously mentioned, CO is adsorbed on Pt both linearly (CO_L) and bridge-bonded (CO_B) since the beginning of the FTIR experiments. The amount of CO_L reaches a maximum between 0.60 and 0.65 V, after which it gradually decreases, while the amount of CO_B remains fairly constant after the CO_L peak. This observation is significantly different from the behavior observed for the GEOR in acidic media, where no band corresponding to CO adsorption on Pt is observed above 0.6 V, because its oxidation to CO_2 is faster than its accumulation on the electrode surface[46]. In the Pt-Bi catalyst, the current is mostly due to production of glycerate and carbonate (fig. 24), with a small contribution from glycolate and formate ions at high potentials (0.75 – 0.85 V). The current density increased considerably after the Bi modification, as well as the amount of glycerate generated. Besides this increase in glycerate production, the reaction pathways that lead to CO formation on Pt were completely blocked by Bi modification, seen by the absence of the CO_L and CO_B bands on the FTIR spectra.

The [CO_3^{2-}]/[Glycerate] ratio is much higher in the clean Pt electrode, indicating that the Bi adatoms hinders the C-C bond breaking. At higher potentials (0.75 – 0.85 V), glycolate and formate were detected by HPLC, thus this hindrance is also influenced by the electrode potential. Thus, the combination of our FTIR and HPLC results indicate that the currents observed in fig. 24 are primarily due to the complete oxidation of GOH to CO_3^{2-} and glycerate, in the absence of the adatom, and to glycerate, glycolate and formate in the Pt-Bi catalyst.

Based on our observations, and on the scheme proposed by Garcia and col.[53,75], we propose the scheme below for the GEOR in alkaline media on the Pt and Pt-Bi catalysts.

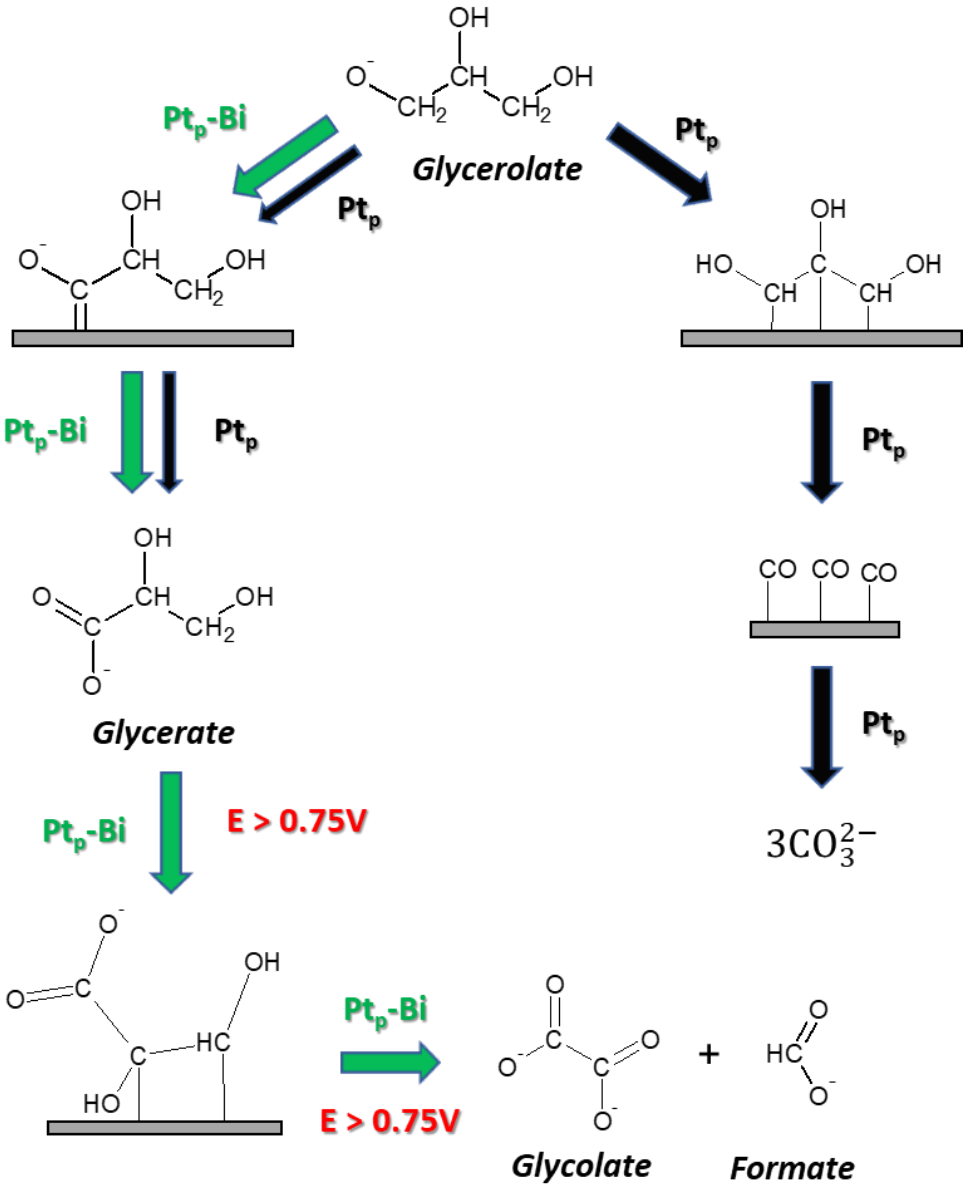

Scheme 5: Proposed reaction scheme for the GEOR in alkaline media in both clean (black) and Bi-modified (green) Pt electrodes.

In our proposal, the main active species is the glycerolate anion, originated from GOH deprotonation in alkaline media, according to reaction (7). This ion may bind through one or more carbons, in one or more steps. Due to a steric effect (availability of adjacent Pt sites) the glycerolate only forms multiple bonds on a clean Pt electrode (C_1-C_2-C_3, C_1-C_2 or C_1-C_3), while on Pt-Bi only single-bonded intermediates are allowed (adsorbing on either the C_1 or C_2 carbons). This happens because our

electrode is completely covered by Bi adatoms, therefore there is a low probability of adjacent vacant Pt sites for the formation of multiple-bonded intermediates.

Garcia and col.[75] have shown that the C_1-C_2 intermediate on Pt(111) leads to oxidation of the secondary carbon, generating either di-hydroxyacetone or glyceraldehyde, while the C_1-C_3 intermediate is inactive on both Pt(111) and Pt(100). Since we could not detect di-hydroxyacetone from the HPLC experiments, and its identification from FTIR spectra is inconclusive due to band superimposition (cf. fig. S3), the C_1-C_2 intermediate was ruled out in our proposal, leaving only the triple-bonded intermediate as the viable reaction pathway. The triple-bonded intermediate suffers C-C bond breaking, generating adsorbed CO (probably in multiple reaction steps), which is further oxidized into carbonate.

An intermediate with a single bond is formed on both catalysts. Since we were unable to detect di-hydroxyacetone, the intermediate bonded through the secondary hydroxyl group was ruled out from this proposal, leaving only the intermediate formed from the primary carbon. The glycerolate adsorbs on the electrode surface through the $-\mathrm{CH_2O^-}$ group, as it is more reactive than $-\mathrm{CH_2OH}$. The fact that glycerate is produced at a much higher rate in Pt-Bi than in Pt indicates that this intermediate reacts faster in the presence of Bi or that higher amounts of the intermediate are being formed on the catalyst surface, or both at the same time.

Lastly, at high potentials (E > 0.75 V), glycolate and formate may be generated from dissociation of the glycerate ion, which would adsorb through its unoxidized carbons on the catalyst surface. This intermediate would then suffer C-C bond breaking, and the carbons would be oxidized, likely in multiple reaction steps. As changes in the Bi adlayer happen during potential cycling (fig. 13), a rearrangement of the Bi adlayer could be occurring at high potentials, allowing adsorption of the glycerate ion and its further oxidation to glycolate and formate. Carbonate may be generated on Pt-Bi through further oxidation of the formate and glycolate ion, as the $\mathrm{CO_3^{2-}}$ band is detected at the same time as the 1720 cm^{-1} band, associated to glycolate, as well as the potential range in which glycolate and formate are detected from HPLC measurements.

5. Conclusions

We have investigated the impact of adatom modification in the activity of Pt and Au electrodes towards the GEOR. The Au_{poly} electrode is deactivated by Pb, Bi or Cu, probably due to the inhibition of the Au(OH) species on the electrode surface.

The Pt electrode also showed deactivation after Cu deposition. On the other hand, the modification with Bi significantly enhance the electrode activity.

The GEOR showed a fivefold increase in current density when 10^{-5} M Bi_2O_3 was added to the electrolye solution. By using FTIR and HPLC, we demonstrated that the presence of Bi inhibited the formation of CO (a poisoning intermediate) and sped up the reaction pathway towards the production of glyceric acid.

Based on our results and on previous papers, we propose two reaction intermediates for the reaction. In the first, the glycerolate adsorbs on the Pt surface through a double bond on the $-CH_2O^-$ group, leading to glyceric acid formation. In the second intermediate, the glyceric acid adsorbs on the electrode surface through the other two carbons, leading to C – C bond breaking, generating glycolic acid and formic acid.

6. Perspectives

In the next step of this work, we will publish our results for the GEOR in alkaline media for the Pt-Bi catalyst.

During the course of this work, we also investigated the Pt-Pb system, and obtained similar results to the PtBi catalyst, while observing a further reduction to the oxidation onset potential. Due to time constraints, we were not able to finish the data treatment and discussion for this catalyst, therefore it was not included into the final version. This system will also be evaluated by a combination of electrochemical, spectroscopic and chromatographic techniques.

We are also investigating the PtBi catalyst using platinum single crystals of the main crystallographic orientations, (111), (110) and (100), both organized and disturbed surfaces[50]. We have concluded the electrochemical measurements for those systems, and the next step is to use a combination of HPLC and FTIR to understand the changes in activity and reaction pathways.

Lastly, we will perform *in-situ* X-ray absorption experiments (*in-situ* XANES and EXAFS) on both Pt-Bi and Pt-Pb catalyst, using spherical Pt nanoparticles to simulate a polycrystalline electrode. From the literature, we know that Bi lowers the work function of Pt(111)[60] however this was performed using low-energy electron diffraction (LEED) *ex-situ*, very different from our experimental conditions. With these experiments, we aim to understand the electronic effect of Pb and Bi on the activity of the Pt catalyst.

7. References

(1) World Energy Council. World Energy Resources 2016. *World Energy Resour. 2016* **2016**, 1–33.

(2) Katryniok, B.; Kimura, H.; Skrzyńska, E.; Girardon, J.-S.; Fongarland, P.; Capron, M.; Ducoulombier, R.; Mimura, N.; Paul, S.; Dumeignil, F. Selective Catalytic Oxidation of Glycerol: Perspectives for High Value Chemicals. *Green Chem.* **2011**, *13* (8), 1960.

(3) Ciriminna, R.; Pina, C. Della; Rossi, M.; Pagliaro, M. Understanding the Glycerol Market. *Eur. J. Lipid Sci. Technol.* **2014**, *116* (10), 1432–1439.

(4) Serrano-Ruiz, J. C.; Luque, R.; Sepúlveda-Escribano, A. Transformations of Biomass-Derived Platform Molecules: From High Added-Value Chemicals to Fuels via Aqueous-Phase Processing. *Chem. Soc. Rev.* **2011**, *40* (11), 5266.

(5) Zhang, Z.; Xin, L.; Li, W. Supported Gold Nanoparticles as Anode Catalyst for Anion-Exchange Membrane-Direct Glycerol Fuel Cell. *Int. J. Hydrogen Energy* **2012**, *37* (11), 9393–9401.

(6) Zhang, Z.; Xin, L.; Qi, J.; Chadderdon, D. J.; Li, W. Supported Pt, Pd and Au Nanoparticle Anode Catalysts for Anion-Exchange Membrane Fuel Cells with Glycerol and Crude Glycerol Fuels. *Appl. Catal. B Environ.* **2013**, *136–137*, 29–39.

(7) Qi, J.; Xin, L.; Zhang, Z.; Sun, K.; He, H.; Wang, F.; Chadderdon, D.; Qiu, Y.; Liang, C.; Li, W. Surface Dealloyed PtCo Nanoparticles Supported on Carbon Nanotube: Facile Synthesis and Promising Application for Anion Exchange Membrane Direct Crude Glycerol Fuel Cell. *Green Chem.* **2013**, *15* (5), 1133.

(8) Martins, C. A.; Fernández, P. S.; Camara, G. A. Alternative Uses for Biodiesel Byproduct: Glycerol as Source of Energy and High Valuable Chemicals. In *Increased Biodiesel Efficiency*; Trindade, M., Ed.; Springer: Cham, 2018; pp 159–186.

(9) Simões, M.; Baranton, S.; Coutanceau, C. Electrochemical Valorisation of Glycerol. *ChemSusChem* **2012**, *5* (11), 2106–2124.

(10) Coutanceau, C.; Baranton, S. Electrochemical Conversion of Alcohols for

Hydrogen Production: A Short Overview. *Wiley Interdiscip. Rev. Energy Environ.* **2016**, *5* (4), 388–400.

(11) Simões, M.; Baranton, S.; Coutanceau, C. Electro-Oxidation of Glycerol at Pd Based Nano-Catalysts for an Application in Alkaline Fuel Cells for Chemicals and Energy Cogeneration. *Appl. Catal. B Environ.* **2010**, *93* (3–4), 354–362.

(12) Crotti, C.; Farnetti, E. Selective Oxidation of Glycerol Catalyzed by Iron Complexes. *J. Mol. Catal. A Chem.* **2015**, *396*, 353–359.

(13) Kwon, Y.; Birdja, Y.; Spanos, I.; Rodriguez, P.; Koper, M. T. M. Highly Selective Electro-Oxidation of Glycerol to Dihydroxyacetone on Platinum in the Presence of Bismuth. *ACS Catal.* **2012**, *2* (5), 759–764.

(14) Zhang, Y.; Zhang, N.; Tang, Z.-R.; Xu, Y.-J. Identification of Bi2WO6 as a Highly Selective Visible-Light Photocatalyst toward Oxidation of Glycerol to Dihydroxyacetone in Water. *Chem. Sci.* **2013**, *4* (4), 1820.

(15) Garcia, R.; Besson, M.; Gallezot, P. Chemoselective Catalytic Oxidation of Glycerol with Air on Platinum Metals. *Appl. Catal. A, Gen.* **1995**, *127* (1–2), 165–176.

(16) Lakshmanan, P.; Upare, P. P.; Le, N.-T.; Hwang, Y. K.; Hwang, D. W.; Lee, U.-H.; Kim, H. R.; Chang, J.-S. Facile Synthesis of CeO2-Supported Gold Nanoparticle Catalysts for Selective Oxidation of Glycerol into Lactic Acid. *Appl. Catal. A Gen.* **2013**, *468*, 260–268.

(17) Porta, F.; Prati, L. Selective Oxidation of Glycerol to Sodium Glycerate with Gold-on-Carbon Catalyst: An Insight into Reaction Selectivity. *J. Catal.* **2004**, *224* (2), 397–403.

(18) Carrettin, S.; McMorn, P.; Johnston, P.; Griffin, K.; Hutchings, G. J. Selective Oxidation of Glycerol to Glyceric Acid Using a Gold Catalyst in Aqueous Sodium Hydroxide. *Chem. Commun. (Camb).* **2002**, No. 7, 696–697.

(19) Thia, L.; Xie, M.; Liu, Z.; Ge, X.; Lu, Y.; Fong, W. E.; Wang, X. Copper-Modified Gold Nanoparticles as Highly Selective Catalysts for Glycerol Electro-Oxidation in Alkaline Solution. *ChemCatChem* **2016**, *8* (20), 3272–3278.

(20) Zhang, Z.; Xin, L.; Qi, J.; Chadderdon, D. J.; Sun, K.; Warsko, K. M.; Li, W.

Selective Electro-Oxidation of Glycerol to Tartronate or Mesoxalate on Au Nanoparticle Catalyst via Electrode Potential Tuning in Anion-Exchange Membrane Electro-Catalytic Flow Reactor. *Appl. Catal. B Environ.* **2014**, *147*, 871–878.

(21) Kwon, Y.; Schouten, K. J. P.; Koper, M. T. M. Mechanism of the Catalytic Oxidation of Glycerol on Polycrystalline Gold and Platinum Electrodes. *ChemCatChem* **2011**, *3* (7), 1176–1185.

(22) Kahyaoglu, A.; Beden, B.; Lamy, C. Oxydation Electrocatalitique Du Glycerol Sur Electrodes d'or et de Platine En Milieu Aqueux. *Electrochim. Acta* **1984**, *29* (10), 1489–1492.

(23) Beden, B.; Çetin, I.; Kahyaoglu, A.; Takky, D.; Lamy, C. Electrocatalytic Oxidation of Saturated Oxygenated Compounds on Gold Electrodes. *J. Catal.* **1987**, *104* (1), 37–46.

(24) Kwon, Y.; Koper, M. T. M. Combining Voltammetry with HPLC: Application to Electro-Oxidation of Glycerol. *Anal. Chem.* **2010**, *82* (13), 5420–5424.

(25) Pletcher, D.; Walsh, F. C. *Industrial Electrochemistry*, 2nd ed.; Springer Netherlands: Dordrecht, 1993.

(26) Souza, M. B. C. de; Fernández, P. S.; Solla-Gullón, J. Adatom Decorated Shape-Controlled Metal Nanoparticles: Advanced Electrocatalysts for Energy Conversion. *Curr. Opin. Electrochem.* **2018**.

(27) Solla-Gullón, J.; Vidal-Iglesias, F. J.; Feliu, J. M. Shape Dependent Electrocatalysis. *Annu. Reports Sect. "C" (Physical Chem.* **2011**, *107*, 263.

(28) Perales-Rondón, J. V.; Solla-Gullón, J.; Herrero, E.; Sánchez-Sánchez, C. M. Enhanced Catalytic Activity and Stability for the Electrooxidation of Formic Acid on Lead Modified Shape Controlled Platinum Nanoparticles. *Appl. Catal. B Environ.* **2017**, *201*, 48–57.

(29) Busó-Rogero, C.; Solla-Gullón, J.; Vidal-Iglesias, F. J.; Herrero, E.; Feliu, J. M. Adatom Modified Shape-Controlled Platinum Nanoparticles towards Ethanol Oxidation. *Electrochim. Acta* **2016**, *196*, 270–279.

(30) Herrero, E.; Fernandez-Vega, A.; Feliu, J. M.; Aldaz, A. Poison Formation

Reaction from Formic Acid and Methanol on Pt(111) Electrodes Modified by Irreversibly Adsobed Bi and As. *J. Electroanal.Chem* **1993**, *350*, 73–88.

(31) Clavilier, J.; Femandez-Vega, A.; Feliu, J. M.; Aldaz, A. Heterogeneous Electrocatalysis on Well Defined Platinum Surfaces Modified by Controlled Amounts of Irreversibly Adsorbed Adatoms. Part III. Formic Acid Oxidation on the Pt(100)-Bi System. *J. Electroanal. Chem. Interfacial Electrochem.* **1989**, *261* (1), 113–125.

(32) Clavilier, J.; Fernandez-Vega, A.; Feliu, J. M.; Aldaz, A. Heterogeneous Electrocatalysis on Well Defined Platinum Surfaces Modified by Controlled Amounts of Irreversibly Adsorbed Adatoms. Part I. Formic Acid Oxidation on the Pt(111)-Bi System. *J. Electroanal. Chem. Interfacial Electrochem.* **1989**, *258* (1), 89–100.

(33) Budevski, E.; Staikov, G.; Lorenz, W. J. *Electrochemical Phase Formation and Growth*, 1st ed.; Budevski, E., Staikov, G., Lorenz, W. J., Eds.; Wiley-VCH Verlag GmbH: Weinheim, Germany, 1996.

(34) Oviedo, O. A.; Reinaudi, L.; Garcia, S.; Leiva, E. P. M. *Underpotential Deposition*, 1st ed.; Scholz, F., Ed.; Monographs in Electrochemistry; Springer International Publishing: Cham, 2016.

(35) Bard, A. J.; Faulkner, L. R. *Electrochemical Methods - Fundamentals and Applications*, 2nd ed.; Harris, D., Swain, E., Robey, C., Aiello, E., Eds.; John Wiley & Sons, Inc: New York, NY, 2000.

(36) Lide, D. R. *CRC Handbook of Chemistry and Physics.*, 90th ed.; Lide, D. R., Ed.; CRC Press (Taylor and Francis Group): Boca Raton, FL, 2009.

(37) Levine, I. N. *Physical Chemistry*, 6th ed.; Hodge, T. L., Oberbroeckling, S. R., Eds.; McGraw-Hill Education: New York, NY, 2008.

(38) Shah, R. K. Introduction to Fuel Cells. *Recent Trends Fuel Cell Sci. Technol.* **2007**, No. 1, 1–9.

(39) Avramov-Ivić, M. L.; Leger, J. M.; Lamy, C.; Jović, V. D.; Petrović, S. D. The Electro-Oxidation of Glycerol on the Gold(100)-Oriented Single-Crystal Surface and Poly Crystalline Surface in 0.1 M NaOH. *J. Electroanal. Chem.* **1991**, *308*,

309–317.

(40) Jeffery, D. Z.; Camara, G. A. The Formation of Carbon Dioxide during Glycerol Electrooxidation in Alkaline Media: First Spectroscopic Evidences. *Electrochem. commun.* **2010**, *12* (8), 1129–1132.

(41) Kwon, Y.; Lai, S. C. S.; Rodriguez, P.; Koper, M. T. M. Electrocatalytic Oxidation of Alcohols on Gold in Alkaline Media: Base or Gold Catalysis? *J. Am. Chem. Soc.* **2011**, *133* (18), 6914–6917.

(42) Birdja, Y. Y.; Koper, M. T. M. The Importance of Cannizzaro-Type Reactions during Electrocatalytic Reduction of Carbon Dioxide. *J. Am. Chem. Soc.* **2017**, *139* (5), 2030–2034.

(43) Shi, X.; Simpson, D. E.; Roy, D. The Role of Chemisorbed Hydroxyl Species in Alkaline Electrocatalysis of Glycerol on Gold. *Phys. Chem. Chem. Phys.* **2015**, *17* (17), 11432–11444.

(44) Enea, O.; Ango, J. P. Molecular Structure Effects in Electrocatalysis-I. Oxidation of Polyols (C2-C6) on Pt and Au Electrodes. *Electrochim. Acta* **1989**, *34* (3–4), 391–397.

(45) Kwon, Y.; Hersbach, T. J. P.; Koper, M. T. M. Electro-Oxidation of Glycerol on Platinum Modified by Adatoms: Activity and Selectivity Effects. *Top. Catal.* **2014**, *57* (14–16), 1272–1276.

(46) Martins, C. A.; Giz, M. J.; Camara, G. A. Generation of Carbon Dioxide from Glycerol: Evidences of Massive Production on Polycrystalline Platinum. *Electrochim. Acta* **2011**, *56*, 4549–4553.

(47) Fernández, P. S.; Martins, M. E.; Martins, C. A.; Camara, G. A. The Electro-Oxidation of Isotopically Labeled Glycerol on Platinum: New Information on C-C Bond Cleavage and CO2 Production. *Electrochem. commun.* **2012**, *15* (1), 14–17.

(48) Fernández, P. S.; Gomes, J. F.; Angelucci, C. A.; Tereshchuk, P.; Martins, C. A.; Camara, G. A.; Martins, M. E.; Da Silva, J. L. F.; Tremiliosi-Filho, G. Establishing a Link between Well-Ordered Pt(100) Surfaces and Real Systems: How Do Random Superficial Defects Influence the Electro-Oxidation of Glycerol? *ACS*

Catal. **2015**, *5* (7), 4227–4236.

(49) Fernández, P. S.; Tereshchuk, P.; Angelucci, C. A.; Gomes, J. F.; Garcia, A. C.; Martins, C. A.; Camara, G. A.; Martins, M. E.; Da Silva, J. L. F.; Tremiliosi-Filho, G. How Do Random Superficial Defects Influence the Electro-Oxidation of Glycerol on Pt(111) Surfaces? *Phys. Chem. Chem. Phys.* **2016**, *18* (36), 25582–25591.

(50) Fernández, P. S.; Martins, C. A.; Angelucci, C. A.; Gomes, J. F.; Camara, G. A.; Martins, M. E.; Tremiliosi-Filho, G. Evidence for Independent Glycerol Electrooxidation Behavior on Different Ordered Domains of Polycrystalline Platinum. *ChemElectroChem* **2015**, *2* (2), 263–268.

(51) Sandrini, R. M. L. M.; Sempionatto, J. R.; Herrero, E.; Feliu, J. M.; Souza-Garcia, J.; Angelucci, C. A. Mechanistic Aspects of Glycerol Electrooxidation on Pt(111) Electrode in Alkaline Media. *Electrochem. commun.* **2018**, *86* (December 2017), 149–152.

(52) Simões, M.; Baranton, S.; Coutanceau, C. Enhancement of Catalytic Properties for Glycerol Electrooxidation on Pt and Pd Nanoparticles Induced by Bi Surface Modification. *Appl. Catal. B Environ.* **2011**, *110*, 40–49.

(53) Garcia, A. C.; Birdja, Y. Y.; Tremiliosi-Filho, G.; Koper, M. T. M. Glycerol Electro-Oxidation on Bismuth-Modified Platinum Single Crystals. *J. Catal.* **2017**, *346*, 117–124.

(54) Adžić, R. R. Electrocatalysis on Surfaces Modified by Foreign Metal Adatoms. *Isr. J. Chem.* **1979**, *18* (1–2), 166–181.

(55) Climent, V.; García-Arez, N.; Feliu, J. M. Clues for the Molecular-Level Understanding of Electrocatalysis on Single-Crystal Platinum Surfaces Modified Byp-Block Adatoms. In *Fuel Cell Catalysis*; Koper, M. T. M., Wieckowski, A., Eds.; John Wiley & Sons, Inc.: Hoboken, NJ, USA, 2008; pp 209–244.

(56) Clavilier, J.; Feliu, J. M.; Aldaz, A. An Irreversible Structure Sensitive Adsorption Step in Bismuth Underpotential Deposition at Platinum Electrodes. *J. Electroanal. Chem. Interfacial Electrochem.* **1988**, *243* (2), 419–433.

(57) Clavilier, J.; Orts, J. M.; Feliu, J. M.; Aldaz, A. Study of the Conditions for

Irreversible Adsorption of Lead at Pt(h,k,l) Electrodes. *J. Electroanal. Chem.* **1990**, *293* (1–2), 197–208.

(58) Wilde, C. P.; Zhang, M. An Electrochemical Quartz Crystal Microbalance Study of Surface Processes at Pt Electrodes Modified with Bi. *Langmuir* **1994**, *10* (5), 1600–1605.

(59) Schmidt, T. J.; Grgur, B. N.; Behm, R. J.; Markovic, N. M.; Ross, Jr., P. N. Bi Adsorption on Pt(111) in Perchloric Acid Solution: A Rotating Ring–disk Electrode and XPS Study. *Phys. Chem. Chem. Phys.* **2000**, *2* (19), 4379–4386.

(60) Paffett, M. T.; Campbell, C. T.; Taylor, T. N. Adsorption and Growth Modes of Bi on Pt(111). *J. Chem. Phys.* **1986**, *85* (10), 6176–6185.

(61) Schmidt, T. J.; Stamenkovic, V. R.; Lucas, C. A.; Markovic, N. M.; Ross Jr., P. N. Surface Processes and Electrocatalysis on the Pt(Hkl)/Bi-Solution Interface. *Phys. Chem. Chem. Phys.* **2001**, *3* (18), 3879–3890.

(62) Schmidt, T. J.; Stamenkovic, V.; Attard, G. A.; Markovic, N. M.; Ross, P. N. On the Behavior of Pt(111)-Bi in Acid and Alkaline Electrolytes. *Langmuir* **2001**, *17* (24), 7613–7619.

(63) Van der Horst, C.; Silwana, B.; Iwuoha, E.; Somerset, V. Synthesis and Characterization of Bismuth-Silver Nanoparticles for Electrochemical Sensor Applications. *Anal. Lett.* **2015**, *48* (8), 1311–1332.

(64) Blais, S.; Jerkiewicz, G.; Herrero, E.; Feliu, J. M. New Insight into the Electro-Oxidation of the Irreversibly Chemisorbed Bismuth on Pt(111) through Temperature-Dependent Research. *J. Electroanal. Chem.* **2002**, *519* (1–2), 111–122.

(65) Friebel, D.; Mbuga, F.; Rajasekaran, S.; Miller, D. J.; Ogasawara, H.; Alonso-Mori, R.; Sokaras, D.; Nordlund, D.; Weng, T.-C. C.; Nilsson, A. Structure, Redox Chemistry, and Interfacial Alloy Formation in Monolayer and Multilayer Cu/Au(111) Model Catalysts for CO2 Electroreduction. *J. Phys. Chem. C* **2014**, *118* (15), 7954–7961.

(66) Rath, D. L. Studies of the Electrode Resistance in the Electrochemical Cell. *J. Electroanal. Chem.* **1983**, *150* (1–2), 521–534.

(67) Deakin, M. R.; Melroy, O. Underpotential Metal Deposition on Gold, Monitored in Situ with a Quartz Crystal Microbalance. *J. Electroanal. Chem.* **1988**, *239*, 321–331.

(68) Schultze, J. W.; Dickertmann, D. Potentiodynamic Desorption Spectra of Metallic Monolayers of Cu, Bi, Pb, Tl, and Sb Adsorbed at (111), (100), and (110) Planes of Gold Electrodes. *Surf. Sci.* **1976**, *54* (2), 489–505.

(69) Avramov-Ivić, M.; Léger, J. M.; Beden, B.; Hahn, F.; Lamy, C. Adsorption of Glycerol on Platinum in Alkaline Medium: Effect of the Electrode Structure. *J. Electroanal. Chem.* **1993**, *351* (1–2), 285–297.

(70) Chang, S. C.; Weaver, M. J. In Situ Infrared Spectroscopy of Carbon Monoxide Adsorbed at Ordered Platinum(100)-Aqueous Interfaces: Double-Layer Effects upon the Adsorbate Binding Geometry. *J. Phys. Chem.* **1990**, *94* (12), 5095–5102.

(71) Cadle, S. H.; Bruckenstein, S. Ring-Disk Electrode Study of the Reduction of Bismuth on Platinum. *Anal. Chem.* **1972**, *44* (12), 1993–2001.

(72) González-Cobos, J.; Baranton, S.; Coutanceau, C. A Systematic in Situ Infrared Study of the Electrooxidation of C3 Alcohols on Carbon-Supported Pt and Pt–Bi Catalysts. *J. Phys. Chem. C* **2016**, *120* (13), 7155–7164.

(73) Schnaidt, J.; Heinen, M.; Denot, D.; Jusys, Z.; Jürgen Behm, R. Electrooxidation of Glycerol Studied by Combined in Situ IR Spectroscopy and Online Mass Spectrometry under Continuous Flow Conditions. *J. Electroanal. Chem.* **2011**, *661* (1), 250–264.

(74) Ferreira, R. S.; Janete Giz, M.; Camara, G. A. Influence of the Local PH on the Electrooxidation of Glycerol on Palladium-Rhodium Electrodeposits. *J. Electroanal. Chem.* **2013**, *697*, 15–20.

(75) Garcia, A. C.; Kolb, M. J.; Van Nierop Y Sanchez, C.; Vos, J.; Birdja, Y. Y.; Kwon, Y.; Tremiliosi-Filho, G.; Koper, M. T. M. Strong Impact of Platinum Surface Structure on Primary and Secondary Alcohol Oxidation during Electro-Oxidation of Glycerol. *ACS Catal.* **2016**, *6* (7), 4491–4500.

8. Appendix

8.1. Determination of theoretical cell voltages

Table 2: Thermodynamic data used. Extracted from ref [37].

Chemical compound	$\Delta H°_f (k\,J.mol^{-1})$	$\Delta G°_f (k\,J.mol^{-1})$	$S°\ (J/mol.K)$
$H_{2(g)}$	0	0	130.684
H_2O_l	-285.83	-237.129	69.91
$CO_3^{2-}{}_{(aq)}$	-677.14	-527.81	56.9
OH_{aq}^-	-229.994	-157.224	-10.75
$C_{(graphite)}$	0	0	5.74
$O_{2(g)}$	0	0	205.138
$Glycerol_{(l)}$	-669.6	-	206.3

Using the data in Table 2, $\Delta G°_{f,Glycerol(l)}$ is determined using the equations below:

$$3C_{(graphite)} + \frac{3}{2}O_{2(g)} + \frac{4}{2}H_{2(g)} \rightarrow Glycerol_{(l)} \quad (13)$$

$$\Delta S°_{f,Glycerol(l)} = S°_{Glycerol(l)} - \left[3S°_{C_{graphite}} + \frac{3}{2}S°_{O_{2(g)}} + \frac{4}{2}S°_{H_{2(g)}}\right]$$

$$\Delta S°_{f,Glycerol(l)} = -379.995\,J/mol.K$$

$$\Delta G°_{f,Glycerol(l)} = \Delta H°_{f,Glycerol(l)} - T \cdot \Delta S°_{f,Glycerol(l)}$$

$$\Delta G°_{f,Glycerol(l)} = -556.361\ \mathrm{k\,J/mol}$$

From reaction (3), $\mathrm{E}^{\circ}_{\mathrm{EC,GOH}}$ is determined as follows:

$$CH_2OH - CHOH - CH_2OH + 6OH^- \rightarrow 3CO_3^{2-} + 7H_2 \quad (3)$$

$$\Delta G°_r = 7\,\Delta G°_{f,H_{2(g)}} + 3\,\Delta G°_{CO_3^{2-}{}_{(aq)}} - \left[6\,\Delta G°_{f,O_{2(g)}} + \Delta G°_{f,Glycerol(l)}\right]$$

$$\Delta G^{\circ}{}_r = -83.605\ k\,J/mol$$

$$\mathrm{E}^{\circ}_{\mathrm{EC,GOH}} = -\frac{\Delta G^{\circ}{}_r}{nF} = +0.062\ V$$

For a water electrolyzer, the reactions involved are

$$2OH^-_{(aq)} \rightarrow \tfrac{1}{2}O_{2(g)} + H_2O_{(l)} + 2e^- \quad (14)$$

$$2H_2O + 2e^- \rightarrow H_2 + 2OH^- \quad (2)$$

$$H_2O_{(l)} \rightarrow H_{2(g)} + \tfrac{1}{2}O_{2(g)} \quad (15)$$

where reaction (15) represents the overall reaction, and $\mathrm{E}^{\circ}_{\mathrm{EC,H_2}O}$ is determined as follows:

$$\Delta G^{\circ}{}_r = \frac{1}{2}\,\Delta G^{\circ}{}_{f,O_{2(g)}} + \Delta G^{\circ}{}_{f,H_{2(g)}} - \Delta G^{\circ}{}_{f,H_2O_{(l)}}$$

$$\Delta G^{\circ}{}_r = 237.129\ k\,J/mol$$

$$\mathrm{E}^{\circ}_{\mathrm{EC,H_2}O} = -\frac{\Delta G^{\circ}{}_r}{nF} = -1.229\ V$$

Similarly, for a GOH-based fuel cell:

$$CH_2OH - CHOH - CH_2OH + {}^{7}\!/_{2}\,O_2 + 6\,OH^- \rightarrow 3CO_3^{2-} + 7H_2O \quad (5)$$

$$\Delta G^{\circ}{}_r = 7\,\Delta G^{\circ}{}_{f,H_2O_{(l)}} + 3\,\Delta G^{\circ}{}_{CO_3^{2-}{}_{(aq)}} - \left[6\,\Delta G^{\circ}{}_{f,OH^-_{(aq)}} + \frac{7}{2}\Delta O_{2(g)} + \Delta G^{\circ}{}_{f,Glycerol(l)}\right]$$

$$\Delta G^{\circ}{}_r = -1743.508\ k\,J/mol$$

$$\mathrm{E}^{\circ}_{\mathrm{FC,GOH}} = -\frac{\Delta G^{\circ}{}_r}{nF} = +1.291\ V$$

For a H_2/O_2 fuel cell:

$$H_{2(g)} + 2OH^-_{(aq)} \rightarrow 2H_2O_{(l)} + 2e^- \quad (16)$$

$${}^{1}\!/_{2}\,O_2 + H_2O + 2e^- \rightarrow 2\,OH^- \quad (4)$$

$$H_{2(g)} \rightarrow \tfrac{1}{2}O_{2(g)} \rightarrow H_2O_{(l)} \quad (17)$$

$$\Delta G^{\circ}{}_r = \Delta G^{\circ}{}_{f,H_2O_{(l)}} - \left[\frac{1}{2}\,\Delta G^{\circ}{}_{f,O_{2(g)}} + \Delta G^{\circ}{}_{f,H_{2(g)}}\right]$$

$$\Delta G^{\circ}{}_{r} = -237.129\ k\,J/mol$$

$$\mathrm{E}^{\circ}_{\mathrm{FC,H_2/O_2}} = -\frac{\Delta G^{\circ}{}_{r}}{nF} = +1.229\ V$$

8.2. Supporting information

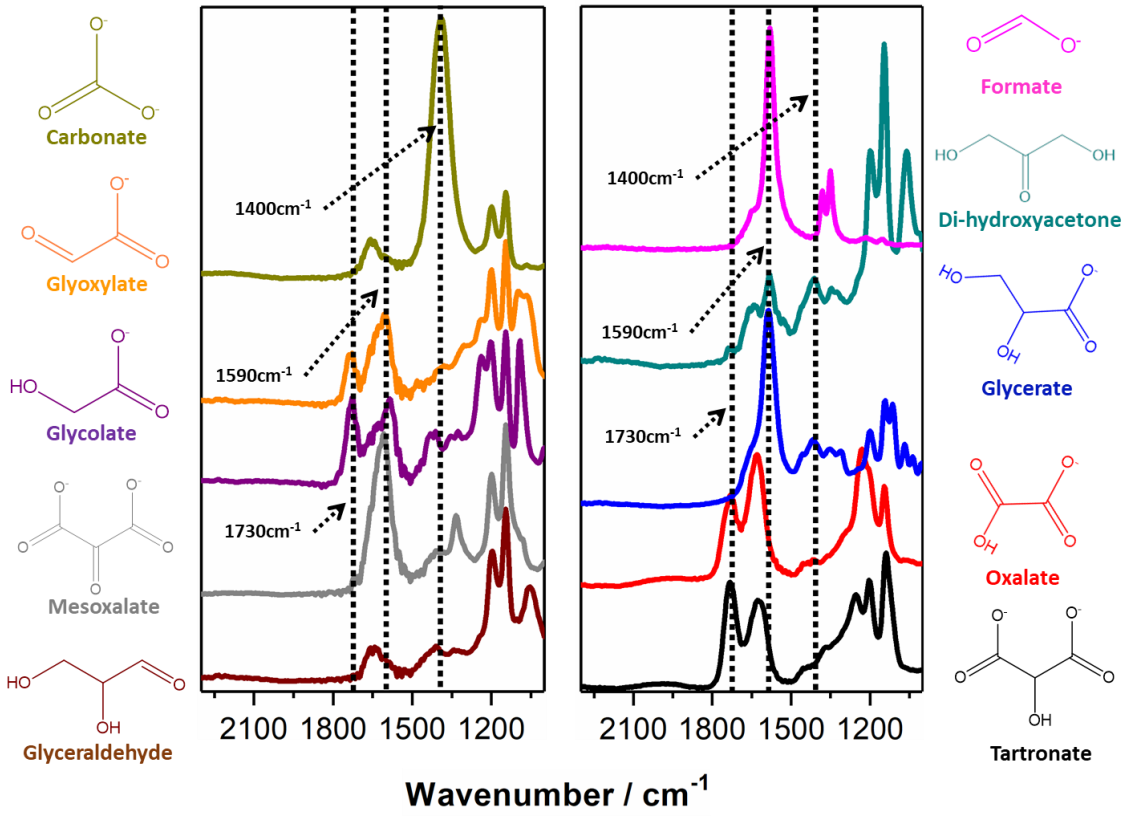

Figure S1: Standard ATR spectra for the identification of the different oxidation products. Each spectrum was recorded from a solution of 0.1 M NaOH + 1 mM of the analyte.

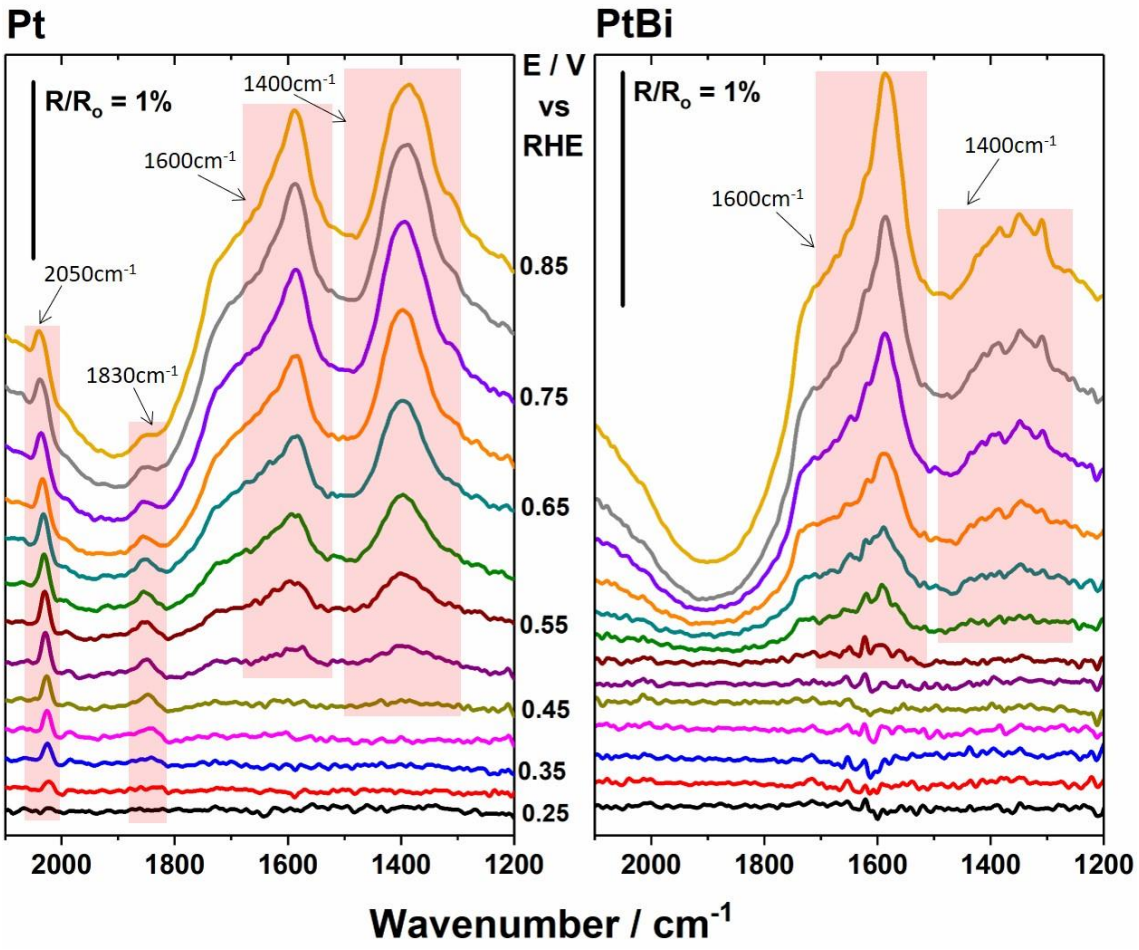

Figure S2: Potential-dependent FTIR spectra for the clean (left) and Bi-modified (right) Pt electrode using H_2O. Electrolyte composition was 0.1 M NaOH + 0.1 M GOH, with 10^{-5} M Bi_2O_3 added for the Bi modification. Scan rate was 2 mV.s^{-1}.

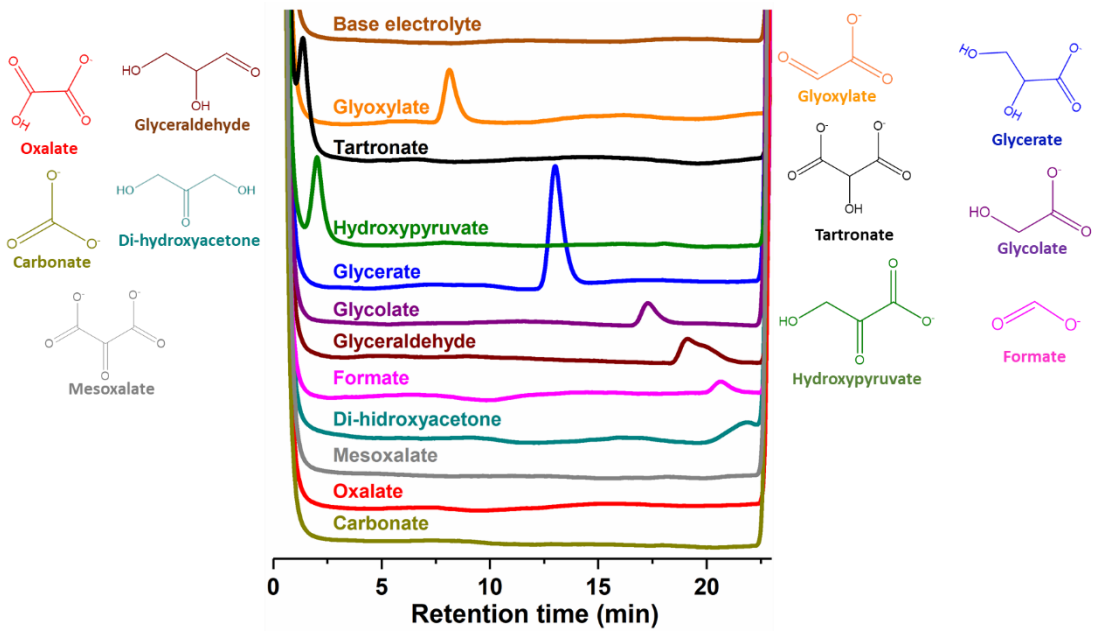

Figure S3: Chromatograms obtained for the identification of several GEOR oxidation products. Each sample consists of the base electrolyte (0.1 M NaOH + 0.1 M GOH + 0.11 H_2SO_4) with 10^{-3} M of the chosen analyte.

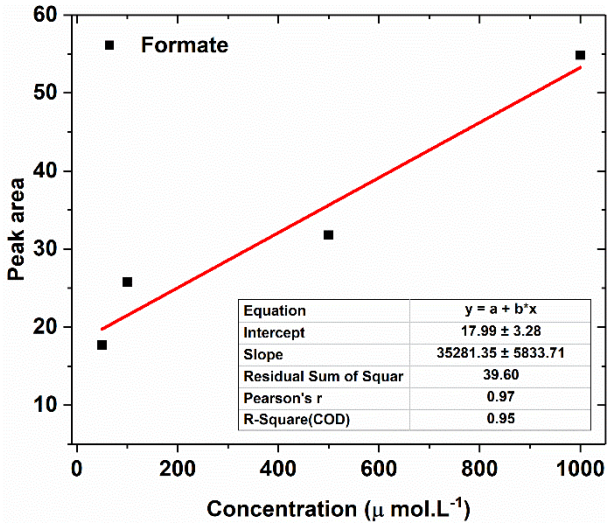

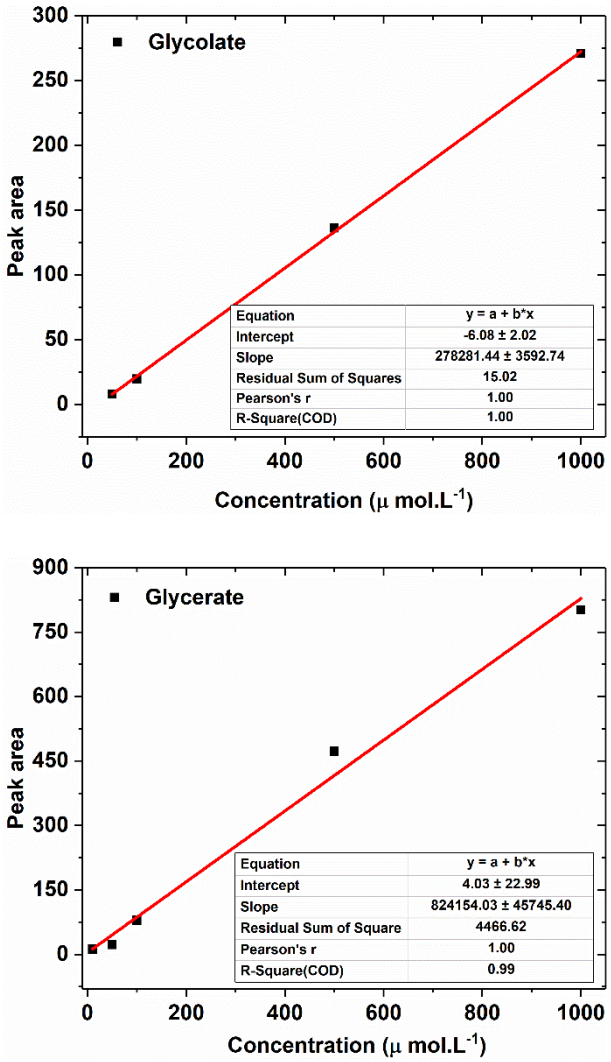

Figure S4: Calibration curves used to quantify formate, glycolate and glycerate ions, from the HPLC measurements.